05/97

PCT WORLD INTELLECTUAL PROPERTY ORGANIZATION
International Bureau

INTERNATIONAL APPLICATION PUBLISHED UNDER THE PATENT COOPERATION TREATY (PCT)

(51) International Patent Classification 6 : A61B 17/00 | A1

(11) International Publication Number: **WO 98/07373**

(43) International Publication Date: 26 February 1998 (26.02.98)

(21) International Application Number: PCT/US97/14760

(22) International Filing Date: 21 August 1997 (21.08.97)

(30) Priority Data:

08/711,289	21 August 1996 (21.08.96)	US
60/034,084	23 December 1996 (23.12.96)	US
60/045,453	1 May 1997 (01.05.97)	US

(81) Designated States: AU, CA, JP, US, European patent (AT, BE, CH, DE, DK, ES, FI, FR, GB, GR, IE, IT, LU, MC, NL, PT, SE).

Published
With international search report.

(71) Applicant *(for all designated States except US)*: BRIGHAM & WOMEN'S HOSPITAL [US/US]; 75 Francis Street, Boston, MA 02115 (US).

(72) Inventor; and
(75) Inventor/Applicant *(for US only)*: HYNYNEN, Kullervo [FI/US]; 36 Oriole Street, Medfield, MA 02052 (US).

(74) Agent: POWSNER, David, J.; Choate, Hall & Stewart, Exchange Place, 53 State Street, Boston, MA 02109 (US).

(54) Title: METHODS AND APPARATUS FOR DELIVERY OF NONINVASIVE ULTRASOUND BRAIN THERAPY THROUGH INTACT SKULL

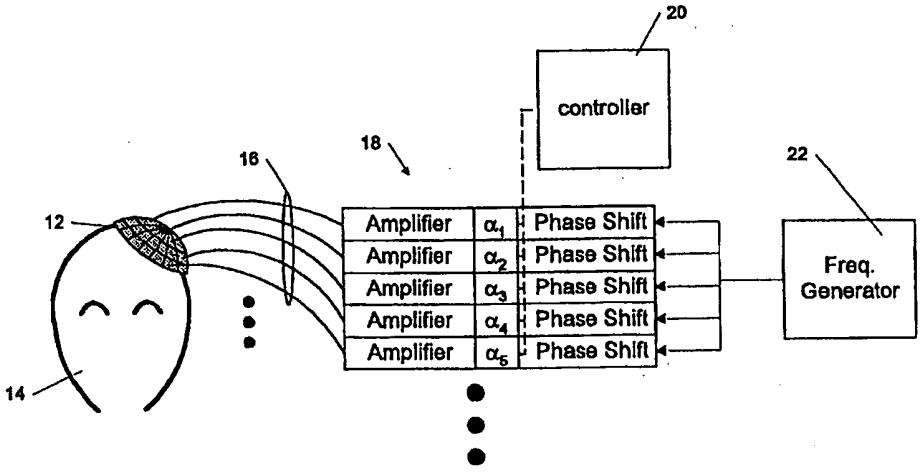

(57) Abstract

Methods and apparatus for delivery of ultrasound to the brain, without requiring removal of portions of the skull, call for transmission of ultrasound with a plurality of transducers (12) aimed to induce cavitation at least at a selected region of the brain. An excitation source (22) is arranged for driving at least selected transducers at differing phases with respect to one another, e.g., to compensate for phase shifts (or phase distortions) effected by the skull on the ultrasound output by each transducer. As a result, the ultrasound waves reaching the selected region from the transducers arrive substantially in phase with one another, e.g., within 90 degrees and preferably 45 degrees, and still more preferably 20 degrees of one another.

FOR THE PURPOSES OF INFORMATION ONLY

Codes used to identify States party to the PCT on the front pages of pamphlets publishing international applications under the PCT.

AL	Albania
AM	Armenia
AT	Austria
AU	Australia
AZ	Azerbaijan
BA	Bosnia and Herzegovina
BB	Barbados
BE	Belgium
BF	Burkina Faso
BG	Bulgaria
BJ	Benin
BR	Brazil
BY	Belarus
CA	Canada
CF	Central African Republic
CG	Congo
CH	Switzerland
CI	Côte d'Ivoire
CM	Cameroon
CN	China
CU	Cuba
CZ	Czech Republic
DE	Germany
DK	Denmark
EE	Estonia
ES	Spain
FI	Finland
FR	France
GA	Gabon
GB	United Kingdom
GE	Georgia
GH	Ghana
GN	Guinea
GR	Greece
HU	Hungary
IE	Ireland
IL	Israel
IS	Iceland
IT	Italy
JP	Japan
KE	Kenya
KG	Kyrgyzstan
KP	Democratic People's Republic of Korea
KR	Republic of Korea
KZ	Kazakstan
LC	Saint Lucia
LI	Liechtenstein
LK	Sri Lanka
LR	Liberia
LS	Lesotho
LT	Lithuania
LU	Luxembourg
LV	Latvia
MC	Monaco
MD	Republic of Moldova
MG	Madagascar
MK	The former Yugoslav Republic of Macedonia
ML	Mali
MN	Mongolia
MR	Mauritania
MW	Malawi
MX	Mexico
NE	Niger
NL	Netherlands
NO	Norway
NZ	New Zealand
PL	Poland
PT	Portugal
RO	Romania
RU	Russian Federation
SD	Sudan
SE	Sweden
SG	Singapore
SI	Slovenia
SK	Slovakia
SN	Senegal
SZ	Swaziland
TD	Chad
TG	Togo
TJ	Tajikistan
TM	Turkmenistan
TR	Turkey
TT	Trinidad and Tobago
UA	Ukraine
UG	Uganda
US	United States of America
UZ	Uzbekistan
VN	Viet Nam
YU	Yugoslavia
ZW	Zimbabwe

Methods and Apparatus for Delivery of Noninvasive Ultrasound Brain Therapy Through Intact Skull

Sponsorship

The research resulted, at least, in part, from work performed under NCI Research Grant No 46627.

Reference to Related Applications

This application claims the benefit of the filing date of and is a continuation-in-part of copending, commonly assigned United States Patent Application Serial No. 08/711,289, filed August 21, 1996 (Attorney Docket No. 0092664-0008), the teachings of which are incorporated herein by reference. This application also claims the benefit of the filing date of copending United States Provisional Application Serial Nos. 60/034,084 (filed 12/23/96), and 60/045,453 (filed 5/1/97). The teachings of those provisional applications are incorporated herein by reference.

Background of Invention

The invention pertains to medical systems and, more particularly, to methods and apparatus for non-invasive application of focused ultrasound to the brain. The invention can be used, for example, in the diagnosis and treatment of neural ailments.

According to the prior art, treatment of tissues lying at specific locations within the skull are limited to removal or ablation. While these treatments have proven effective for certain localized disorders, such as tumors, they involve delicate, time-consuming procedures that may result in destruction of otherwise healthy tissues. The treatments are generally not appropriate for disorders in which diseased tissue is integrated into healthy tissue, except in instances where destruction of the latter will not unduly effect neurologic function.

The noninvasive nature of ultrasound surgery has special appeal in the brain where it is often desirable to destroy or treat deep tissue volumes without disturbing the healthy tissues.

Focussed ultrasound beams have been used for noninvasive surgery in many other parts of the body. Ultrasound penetrates well through soft tissues and, due to the short wavelengths (1.5 mm at 1 MHz), it can be focused to spots with dimensions of a few millimeters. By heating tumorous or cancerous tissue in the abdomen, for example, it is possible to ablate the diseased portions without significant damage to surrounding healthy tissue.

Notwithstanding the potential benefits of ultrasound diagnostics and therapy of the brain, it has been commonly accepted that ultrasound cannot be applied through the intact skull. Early experiments, for example, showed that ultrasound is strongly attenuated by bone, and that brain tissue damage close to the skull results from the high temperatures caused by the energy loss. Accordingly, all of the ultrasound brain treatments performed so far have required the skull bone to be removed prior to the sonication. This makes the procedure invasive, and expensive with an added risk of complications.

The requirement of surgical removal of the skull has been the main obstacle that has prevented ultrasound therapy to be widely tested in the brain despite the possibility of its clear benefits compared to other techniques. Accordingly, an object of this invention is to provide improved medical methods and apparatus, for diagnosis and therapy of the brain. A more particular object of the invention is to provide improved methods and apparatus for application of ultrasound to the brain.

A more particular object of the invention is to provide such methods and apparatus as do not require removal of portions of the skull, via craniectomy or other such procedures.

Still another object of the invention is to provide such methods and apparatus as can be used to precisely target regions within the brain.

Still yet another object of the invention is to provide such methods and apparatus as can be used to effect heating or other physiologic change at such precisely targeted regions, without effecting substantial change in the surrounding, or other, regions of the brain or skull.

Another object of the invention is to provide such methods and apparatus as can be utilized over a wide range of ultrasonic frequencies.

Still another object of the invention is to provide such methods and apparatus as can be implemented utilizing conventional materials.

Yet still another object of the invention is to provide such methods as can be implemented without excessive expense.

Summary of the Invention

The foregoing and other objects are met by the invention, which provides in one aspect methods and apparatus for delivery of cavitating ultrasound to the brain, without requiring removal of portions of the skull.

Thus, in one aspect, the invention provides an apparatus for delivering ultrasound, through intact skull, to the brain comprising a plurality of transducers and an excitation source for driving each to induce cavitation at least at a selected region of the brain. The excitation source is particularly arranged for driving at least selected transducers at differing phases with respect to one another, e.g., to compensate for phase shifts (or phase distortions) effected by the skull on the ultrasound output by each transducer. As a result, the ultrasound waves reaching the selected region from the transducers arrive substantially in phase with one another, e.g., within 90° and, preferably, within 45° and, still more preferably, within 20° of one another.

The excitation source drives the transducers to deliver ultrasound to the selected region at a frequency ranging from 0.01 MHz to 10 MHz and, preferably, from 0.1 MHz to 2 MHz. Sonication duration for the ultrasound ranges, according to further aspects of the invention, from 100 nanoseconds to 30 minutes. According to still further aspects, the invention provides for delivery of ultrasound to the selected region with continuous wave operation or burst mode operation, where burst mode repetition varies from 0.01 Hz to 1 MHz.

Further aspects of the invention provide an apparatus as described above, in which only a single transducer is used.

Still further aspects of the invention provide methods for operating transducer arrays as described above.

These and other aspects of the invention are evident in the drawings and in the text that follows.

Brief Description of the Drawings

A further understanding of the invention may be attained by reference to the drawings, in which:

Figure 1 depicts an embodiment of the invention and an experimental setup for testing it.

Figure 2 depicts an embodiment of the invention for application of ultrasound to the brain of an animal.

Figure 3 depicts a phased array for application of ultrasound to the brain in accord with one practice of the invention.

Figures 4A-4H illustrate the ultrasound pressure amplitude distribution in water across the focus of a transducer according to the invention at various frequencies, with and without skull sections in front of the transducer.

Figures 5A and 5B illustrate the effect of applying ultrasound in accordance with the invention to brain tissue.

Figures 6A and 6B illustrate phase errors measured at the focus of ultrasound transducer arrays with a piece of skull in front of the transducers.

Figures 7A-7C illustrate the pressure amplitude profiles across the focus of an ultrasound transducer phased array in water, through the bone, and through the bone with phase correction.

Figure 8 illustrates the pressure amplitude distribution along the central axis of an ultrasound transducer array without and with the phase correction.

Figures 9A-9C illustrate the ultrasound pressure amplitude distribution measured across the focus of an ultrasound phased array in water, through skull without phase correction, and through skull with phase correction.

Figure 10 depicts an embodiment of the invention for delivery of cavitating ultrasound to a patient's brain through the skull using a multi-element transducer array.

Figure 11 depicts a method for delivery of cavitating ultrasound to a patient's brain through the skull using a transducer array.

Detailed Description of the Illustrated Embodiment

Discussed below are methods and apparatus according to the invention for noninvasive delivery of ultrasound through intact skull to the brain. These permit ultrasound propagation through skull to effect cavitation, without causing undesired heating of the brain or, more generally, central nervous system (CNS) tissues. These also deliver adequate ultrasound power to ablate tissues, or to otherwise induce changes, at focal points (or regions) within the brain. As used herein, "tissue" refers to fluids, tissues or other components on or within a patient's body.

Figure 10 depicts an apparatus according to the invention for delivery of ultrasound to the brain. The apparatus 10 includes an array of transducers 12 disposed on or near the external surface of the head of a human patient. The array 12 can constitute a single transducer, e.g., a spherically curved piezoelectric bowl of the type described below, though preferably, array 12 comprises a plurality of transducers arranged in a one-, two- or three-dimensional configuration.

Referring to Figure 3, for example, in one embodiment of the invention, array 12 comprises 60 individual piezoelectric ceramic transducers mounted in a bowl of circular cross-section. The transducer elements, which can be, for example, 1 cm^2 piezoelectric ceramic pieces, are mounted in silicone rubber or any other material suitable damping agent for minimizing the mechanical coupling therebetween. Transducer arrays of this type are known in the art, as described, for example in Fan *et al*, "Control of the Necrosed Tissue Volume During Noninvasive Ultrasound Surgery Using a 16-Element Phased Array," Medical Physics, v. 22, pp. 297 *et seq* (1995), a copy of which is filed as an appendix hereto and the teachings of which (e.g., at Figure 1 and the accompanying text) are incorporated herein by reference. The construction of a spherically curved phased array comprising multiple square-element transducers is shown in Figure 1 and the accompanying text of that publication.

In the illustrated embodiment, each transducer of array 12 is independently driven by power and the control elements 18-22 to generate ultrasound for transmission through the patient's skull into the CNS tissues. More particularly, the transducers in array 12 are individually coupled, via coaxial cables 16, to separate channels of a driving system 18. Each channel of that system 18

includes an amplifier and a phase shifter, as shown. A common radio frequency (RF) signal is driven to each channel by radio frequency generator 22. Together, the radio frequency generator 22 and driving system 18 drive the individual transducers of array 12 at the same frequency, but at different phases, so as to transmit a focused ultrasound beam through the patient's skull to a selected region within the brain. Unlike prior art systems, there is no need to remove portions of the skull beneath the array 12, e.g., via craniectomy or other such surgical procedure.

The radio frequency generator 22 can be of any commercially available type. A preferred such generator is available from Stanford Research Systems, Model DS345. The generator is operated in a conventional way so as to generate an excitation signal, which is amplified and phase-shifted by the individual channels of driving system 18, in order to induce the corresponding transducers of array 12 to radiate ultrasound (e.g., in the range 0.01 MHz to 10 MHz).

As illustrated, each channel in the driving system 18 includes a radio frequency amplifier. These can be any RF amplifiers of the type commercially available in the art.

The phase shifting component of each channel of driving system 18 is constructed and operated in the conventional manner known in the art. Particularly, each phase shifter shifts the phase of an incoming RF excitation signal, received from RF generator 22, by an amount α_1, α_2, α_3, etc., as shown in the drawing. These phase shift factors α_1, α_2, α_3, etc., can be pre-stored in the channels of driving system 18 or, preferably, generated by a controller 20. That controller 20 can be a general purpose, or special purpose, digital data processor programmed in a conventional manner in order to generate and apply phase shift factors in accord with the teachings hereof.

The phase shift factors, α_1, α_2, α_3, etc. serve two purposes. The first is to steer the composite ultrasound beam generated by transducer array 12 so that it is focused on a desired region within the patient's brain. The component of each phase shift factor associated with steering is computed in the manner known in the art for steering phased arrays. See, for example, Buchanan *et al*, "Intracavitary Ultrasound Phased Array System," IEEE Transactions Biomedical Engineering, v. 41, pp. 1178-1187, a copy of which is filed as an appendix hereto and the teachings of which are incorporated herein by reference. Array steering, or focusing, is particularly discussed in that article,

for example, at pages 1179-1181 and, more particularly, in the section entitled "Focusing Techniques," the teachings of which are incorporated herein by reference.

The second component of each phase shift factor α_1, α_2, α_3, etc., compensates for phase distortion effected by the skull in the ultrasound ouput by each transducer. In other words, the second component of the phase shift factors compensates for perturbations and distortions introduced by the skull, the skin/skull interface, the dura matter/skull interface, and by variations in the skull thickness. As those skilled in the art will appreciate, the two components that make up the phase shift factor for each channel of the driving system 18 are summed in order to determine the composite phase shift factor for the respective channel.

The phase corrections that constitute the aforementioned second component of each phase shift factor can be determined a number of ways. In one embodiment of the invention, that component is determined from measurements of the thickness of the patient's skull under each transducer in array 12. Such skull thickness measurements can be made using conventional imaging techniques, such as computed tomography (CT) or magnetic resonance imaging (MRI).

In an alternative embodiment, the aforementioned second component of each phase shift factor is determined by placing the array 12 on the patient's head and exciting individual transducers with a short ultrasound pulse. The echo back from the inner surfaces of the skull are monitored by the transducer array 12. The effect of the skull on ultrasound generated by each transducer is determined from those echos in accord with conventionally known relations.

In still further alternative embodiments, the aforementioned second component of each phase shift factor is determined by implanting small hydrophones in the patient's brain. These are used to monitor the phase of the ultrasound generated by each transducer, e.g., in a manner similar to that described below in connection with Figure 1.

In lieu of illustrated components 18-22, the transducer array 12 can be driven by a driving system of the type disclosed in Buchanan *et al*, *supra* e.g. at Figure 2 thereof, the

teachings of which are incorporated herein by reference. Such a driving system would, of course, require modification in accord with the teachings hereof in order to incorporate phase shift factors α_1, α_2, α_3, etc., having first and second components as described herein and above.

Referring to Figure 11, the system 10 is operated as described below in order to deliver ultrasound through the patient's skull to induce cavitation at a desired region of the brain.

In step 24, the transducer array 24 is positioned on the patient's head. This is preferably accomplished in the conventional manner known in the art for insuring ultrasound transmission to the brain. The array is typically positioned over, and as close to, the region in which cavitation is to be induced. However, where intervening or adjacent cranial or CNS tissues might be adversely affected, the array can be positioned elsewhere and focused accordingly.

In step 26, the aforementioned second component of the phase shift factor for each transducer is determined. This is accomplished in the manner described above, e.g., by individual exciting each element of the array and measuring the echo back. The alternative mechanisms described above can also be used to determine those components. Those skilled in the art will appreciate that in instances where the alternative mechanisms are used, they need not be performed after the array is positioned but, can be performed at some other prior time.

In step 28, the remaining components of each transducers' phase shift factor are determined. Particularly, those components associated with steering the array for delivery of ultrasound to the desired region are determined. Such determination is made, as indicated above, in the conventional manner known in the art for steering phased arrays.

In step 30, the array is excited, e.g., by control and driving elements 18-22, to focus ultrasound in the patient's head. As noted throughout, because the invention provides correction for phased distortion induced by the skull, that ultrasound can be supplied directly through the skull without the need for removal of a piece thereof. The ultrasound is applied in doses and timing sufficient to induce cavitation in the desired region, which may be, e.g., from 1 mm^3 - 1 cm^3, or larger. Those skilled in the art will appreciate that ultrasound waves in the frequency

range of 0.01 MHz to 10 MHz and, preferably, from 0.10 MHz to 2 MHz can be applied with sonication duration ranging from 100 nanoseconds to 30 minutes, with continuous wave or burst mode operation. The burst mode repetition varies from 0.01 Hz to 1 MHz.

In embodiments where the transducer array 12 includes only a single transducer, e.g., a 10 cm diameter piezoelectric ceramic element as described elsewhere herein, step 26 is not utilized. In such an embodiment, the "array" is aimed based on its focal point. This is determined as a function of the size, radius of curvature and frequency output of the transducer in the manner known in the art. In a preferred embodiment, these factors are adjusted so that the transducer can be placed directly on the patient's skull, as above. However, where minor corrections are necessary, the transducer can be spaced apart from the skull, as necessary, in order to insure proper positioning of the focal point.

Theory

When an ultrasound beam propagates to a deep target location in the brain part of the energy is reflected back at the skin-skull interface due to the high acoustic mismatch between these two tissues. The propagating wave in the skull suffers attenuation losses due to scattering and absorption. The acoustic mismatch at the bone-dura interface causes part of the remaining wave to reflect back to the skull. The total insertion loss through skull depends on the frequency, and can be, on average, about 10 dB, and 20 dB at 0.5, and 1.5 MHz, respectively. The wave is further attenuated by absorption (about 5 Np/m/MHz) while it travels through the brain to the target volume.

An ultrasound beam delivered to the brain can effect change in CNS tissues and fluids (herein, simply "tissue" or "brain tissue," etc.) by two mechanisms: heating and cavitation. The ultrasound beam can heat the tissue temperature due to energy absorption from the wave resulting in different degrees of thermal damage to the tissue depending on the temperature reached. For exposures of a few seconds, temperatures of above about 60° C are adequate to coagulate proteins and thus, necrose the tissue. The induced temperature elevation during short ultrasound exposures depends mainly on the absorbed power (<q>) although the shape and size of the focal spot can have a significant impact due to thermal conduction. The rate of

temperature rise (dT/dt) at the very beginning of an ultrasound pulse can be calculated from the pressure amplitude of the field (P), as follows:

$$dT/dt = <q>/ \rho c, \qquad [1]$$

where

$$<q> = \alpha P^2/ \rho v \qquad [2]$$

ρ is the density (ρ_b = 1030 kg/m^3 , ρ_s = 1380-1810 kg/m^3) (s= skull, b = brain),

c is the specific heat of the medium (c_b =3.9 kJ/kg/°C ; c_s =2.1-2.7 kJ/kg/°C),

v is the speed of sound, and

α is the amplitude absorption coefficient of the tissue (α_b= 5Np/m/MHz, α_s = 50 Np/m at 0.5 MHz, α_s = 300 Np/m at 1.5 MHz (if all attenuated energy is assumed to be absorbed)).

In order to achieve the same temperature within the target volume as in the skull, the ultrasound beam has to be focused to overcome the difference in the acoustic properties. The square of the pressure amplitude (P^2) is directly proportional to the ultrasound beam area allowing the required area gain (AG) to be calculated from Equations [1] and [2] by making the rates of temperature rise equal in the skull and the brain:

$$AG = (P_b^2/P_s^2) = (\alpha_s/\alpha_b)(\rho_b/\rho_s)^2(v_b/v_s)(c_b/c_s) = 30 \text{ at } 0.5 \text{ MHz} \quad [3]$$

$$= 60 \text{ at } 1.5 \text{ MHz}$$

In addition the area gain has to compensate for the energy loss due to the skull and attenuation in the brain between the skull and the focal point:

$$AG' = (\alpha_i e^{-2\beta x})^{-1} = 13 \text{ at } 0.5 \text{ MHz} \quad [4]$$

$$= 250 \text{ at } 1.5 \text{ MHz}$$

where,

α_i is the insertion loss of skull,

β is the amplitude attenuation coefficient,

f is the frequency and x is the depth in the brain.

The total area gain is the product of these two area gains and is approximately 400 and 15000 at 0.5 MHz and 1.5 MHz, respectively when the focus is located at the depth of 6 cm in the brain. These calculations are first order estimates and do not take into account phase shifts introduced by the variable thickness of the bone or thermal conduction and perfusion effects.

The second mechanism, cavitation requires negative pressure amplitudes that are large enough to form gas bubbles in the tissue. The pressure wave causes the bubbles to expand and then collapse. The collapse of the bubbles causes high temperatures and pressures that can cause direct mechanical damage to the tissue. Cavitation can offer more therapeutic options than thermal exposures of brain. The cavitation threshold in the soft tissues and in bone appears to be similar.

Thus, focusing a cavitation-inducing ultrasound beam overcomes the attenuation losses in the bone and brain, but need not overcome differences in absorption coefficients, as is the case with the heat-inducing exposures. The beam area of cavitation-inducing ultrasound propagating through the skull has to be about 13 and 250 times larger than the focal area at frequencies of 0.5 and 1.5 MHz, respectively. These area gains are 30 and 60 times smaller than the gains required for induction of thermal effects. The cavitation is not influenced by thermal conduction or perfusion effects. Therefore, it is clear that cavitation has significant advantages over the thermal effects. This is particularly true in instances where the ultrasound energy must be delivered to small focal regions that require high frequencies.

Cavitation requires high pressure amplitudes but only short exposure durations, therefore cavitational effects can be induced without significant temperature elevation. For CNS tissues, sonications with durations of only 1 ms are adequate for bubble formation. The required peak intensities at 0.936 MHz during these sonications are measured to be around 4000 Wcm^{-2} and

2000 Wcm^{-2} at 1 ms and 1 s exposures, respectively. Using these intensity values and the average ultrasound attenuation in brain of 5 Np/m and in bone 120 Np/m at 1 MHz, the maximum peak temperature elevation in the brain can be estimated (from equations 1 and 2) to be about 60° C and 0.1° C during the 1 s and 1 ms exposures, respectively. The corresponding temperature elevations in bone, if the focus was in the bone, are 1800° C and 3.6° C. During the sonications the temperature elevation in the bone would be reduced proportionally with the area gain. These values are frequency dependent. For example, bone heating would be about 13° C for 1 ms pulse at 1.5 MHz. This short thermal exposure is below the threshold for tissue damage. Thermal exposures can be further reduced using multiple pulses that can be repeated at a low frequency (for example 0.1 Hz) thus, eliminating a temperature build up.

Examples

In one exemplary embodiment of the invention, which is illustrated in Figure 1, ultrasound was generated using a one-element transducer array having a spherically curved 10 cm diameter piezoelectric ceramic (PZT4) bowl mounted in a plastic holder using silicon rubber. The ceramic had silver or gold electrodes both on the front and back surface. The electrodes were attached to a coaxial cable that was connected to a LC matching network that matched the electrical impedance of the transducer and the cable to the RF amplifier output impedance of 50 ohm and zero phase. The matching circuit was connected to an RF- amplifier (both ENI A240L and A500 were used in the tests). The RF signal was generated by a signal generator (Stanford Research Systems, Model DS345).

The ultrasound pressure wave distributions were measured using needle hydrophones (spot diameter 0.5 and 1 mm) and an amplifier (Precision Acoustics Ltd). The amplified signal was measured and stored by a oscilloscope (Tektronix, model 2431L). The hydrophone was moved by stepper motors in three dimensions under computer control. The pressure amplitudes measured by the oscilloscope were stored by the computer for each location.

A piece of human skull (top part of the head: front to back 18 cm and maximum width 12 cm) was obtained and fixed in formaldehyde. The acoustic properties of formaldehyde fixed

skull and a fresh skull are almost identical. The ultrasound transducer under test was positioned in a water tank the walls and bottom of which were covered by rubber mats to reduce ultrasound reflections. The tank was filled with degassed deionized water. The hydrophone was connected to the scanning frame, and positioned at the focus of the ultrasound field.

Utilizing the setup shown in Figure 1, the embodiment was tested at four different ultrasound frequencies: 0.246 MHz, 0.559 MHz, 1 MHz, and 1.68 MHz. The maximum peak pressure amplitudes achievable through the skull at the focus of the transducer was measured at each frequency. A shock wave hydrophone (Sonic Technologies Inc,) was positioned at the acoustic focus. Bursts of 10-20 cycles were used to separate the acoustic signal from the electrical interference that was picked up by the hydrophone during sonication. Results of the testing are shown in Figures 4A-4H.

Particularly, Figure 4A illustrates the ultrasound pressure amplitude distribution in water at the focal point of the single transducer driven at 0.246 MHz, without the skull section in place. Figure 4B illustrates this same distribution when the skull was positioned in front of the transducer as illustrated in Figure 1. Figures 4C and 4D illustrate the same distributions (i.e., with and without the skull section in place) for a frequency of 0.559 MHz. Figures 4E and 4F illustrate the same distributions for a frequency of 1 MHz. Figures 4G and 4H illustrate the same distributions for a frequency of 1.68 MHz.

To demonstrate that the single-element array of this embodiment delivers sufficient energy to induce tissue damage through the skull, in vivo rabbit experiments were performed. In these experiments a window of about 15x15 mm was created in the top of the skull. The skin was placed over the skull opening and the animal was allowed to recover. A minimum of two weeks after the surgery the animal was anesthetized again and placed on top of a sonication tank as illustrated in figure 2 and the 0.556 MHz transducer was aimed such than the focus was located at 10-15 mm in the brain. The skull piece was positioned in between the traducer and the animal. A thermocouple probe (0.05 mm constantan and copper wires were soldered together at the tip) was placed on the skull bone (on the side of the transducer that is expected to be the hottest location) under a thin layer of connective tissue that was still attached on the skull. Then

10 sonications at the maximum power level for the duration of 0.2 s were repeated with the rate of 1 Hz. The animal position was moved and the sonication repeated four times in the same location with a delay of about 5 min between the sonications to allow the bone temperature to return to the baseline. During the 10 s of pulsed sonication the bone temperature increased from the baseline of about 30° C to maximum of 43° C with rapid decay. After the sonications the rabbit was taken to a MRI scanner and T1, T2 and contrast enhanced scan were performed. After the imaging the animal sacrificed.

Figure 5A is a scan of the rabbit brain illustrating the effect of 10 sonications for the duration of 0.2 seconds, with a pressure amplitude of 8 MPa, repeated at a rate of 1. Hz. During the 10 seconds of pulse sonication, the bone temperature in the rabbit skull peaked from a baseline of about 30° C to a maximum of 43° C, with rapid decay. The Figure is a T2-weighted fast spin echo image across the brain. The arrow in the Figure shows tissue damage at the focal point of the transducer. The skull window on the top of the head is facing down and, thus, the ultrasound beam propagated from bottom up. Figure 4B is identical to Figure 4A, except insofar as it shows the results where the above sonication was repeated four times.

Further embodiments of the invention utilize multi-element phase arrays of the types illustrated in Figures 3 and 10, in lieu of a single transducer. By controlling the phase of the ultrasound wave as a function of transducer location, these embodiments eliminate the phase distortion caused by the skull and thus, allow accurate aiming and use of higher frequencies, thus, permitting application of ultrasound to induce cavitation through the intact skull in regions of 1 mm to 1 cm^3.

Two phased arrays comprising these further embodiments had similar structure and the same driving hardware; the resonant frequency being their only significant difference. The two arrays operated at 0.6 MHz and 1.58 MHz. The radius of curvature of both of the transducers was 10 cm and both of them were cut into approximately 1 cm^2 square elements, as shown in Figure 3. The total number of elements in both arrays was 64 although only 60 were driven in the experiments due to hardware limitations. The ceramic bowl was cut using a diamond wire saw so that the elements were completely separated by a 0.3-0.5 mm kerf. The kerf was filled

with silicone rubber that kept the array elements together and isolated them acoustically. The silicone rubber allowed the transducer elements to vibrate with minimum amount of clamping. Each transducer element was connected to a coaxial cable and a matching circuit that was individually tuned. The arrays were similar to the one described in Fan *et al, supra*, at Figure 1 and the accompanying text, the teachings of which are incorporated herein by reference. The array was driven by an in-house manufactured 64 channel driving system that included an RF amplifier and phase shifter for each channel. The phase and amplitude of the driving signal of each channel was under computer control, as described in Buchanan *et al, supra*, e.g., at Figure 2 and the accompanying text, the teachings of which are incorporated herein by reference.

In addition to phased arrays configured as described herein and shown in the accompanying drawings, phased arrays can also be constructed in accord with the arrangements described and shown in co-pending, commonly assigned patent application 08/747,033, filed November 8, 1996, the teachings of which are incorporated herein by reference.

Using the methodologies and apparatus described above, it is possible to produce a sharp focus through the skull with the single element transducer when the operation frequency was 1 MHz or less. The beams had secondary peaks introduced by the skull but the main peak was the largest. The location of the peak was shifted by the skull by 1-3 mm from the geometric focus, as shown in Figures 4A - 4H. However, the focus was completely obliterated with an operating frequency of 1.67 MHz, as shown in Figure 4H.

The maximum pressure amplitudes achieved at the maximum power output of the amplifier were frequency dependent and are given in the table below. The maximum average pressure amplitude at the frequency of 0.554 MHz was 8.0+/- 0.6 MPa.

Frequency (MHz)	Average Pressure Amplitude (MPa)	P+ (MPa)	P- (MPa)
0.248	3.8	4.2	3.3
0.559	8.0	8.9	7.1
1.0	5.9	6.9	4.5

Figure 5 shows the image across the brain for the first of the sonications and demonstrate tissue damage indicated T2 changes. The tissue damage was also visible in T1 images with and without contrast enhancement.

To measure the phase distortion caused by the skull, a hydrophone was placed in the geometric focus of the array under test. The skull was placed between the array and hydrophone and each transducer element was powered separately in sequence while recording the time difference between the reference signal and the acoustic wave at the focus. This was done with both of the arrays. The phase changes required to correct all of the waves to arrive at the same phase at the focus are plotted in Figure 6.

To investigate the effect of the phase correction the pressure amplitude distributions were measured in water by scanning the needle hydrophone. The main impact of the phase at 0.6 MHz was in the location of the focus which could be corrected back to the geometric focus. This is shown in Figure 7A, which illustrates the pressure amplitude profile across the focus of the 0.6 MHz phased array in water. Figure 7B shows the pressure amplitude profile across the focus through bone. And, Figure 7C shows the pressure amplitude profile through bone when a phase correction according to the invention is used. Figure 8 likewise illustrates the pressure amplitude distribution along the central axis of the array with and without phased correction. The magnitude was reduced to 33 % and 40 % of its water value without and with the phase correction, respectively. The importance of the phase correction was demonstrated more clearly with the higher frequency array. With this array the focus was completely destroyed by the skull

(Figure 9b). However, when phase correction was introduced, the focal spot was returned into its original shape (Figure 9c) with the half-width of the focus of about 1 mm. The insertion of the skull reduced the peak pressure at the focus of the 1.58 MHz array to about 5 % of its water value when phase correction was applied.

The embodiments of the invention discussed above and shown in the drawings provide improved methods and apparatus for neural diagnosis and therapy through application of short, high intensity ultrasound beams that induce cavitation at selected locations within the brain. These and other embodiments can be beneficially used to deliver focused ultrasound beams to the CNS tissues and fluids, thereby, permitting their ablation or other physiological modification. Thus, for example, the embodiments can be used to ablate tumors, cancers and other undesirable tissues in the brain. They can also be used, for example, in connection with the technologies disclosed in copending, commonly-assigned U.S. Patent Application No. 08/711,289 (the teachings of which are incorporated herein by reference) for modification of the blood-brain barrier, e.g., to introduce therapeutic compounds into the brain. Because they do not require that portions of the skull be removed, the embodiments permit the foregoing to be performed noninvasively.

The results also show that adequate ultrasound transmission can be induced through human skull to induce cavitation in vivo. This can be done with single element applicators, e.g., preferably at frequencies less than 1 MHz and at higher frequencies with phased arrays that correct the phase distortion caused by the variable thickness of the skull.

The maximum pressure amplitude of 8 MPa induced through the skull at 0.559 MHz was able to induce cavitation damage in vivo rabbit brain. This value was reached through an area of 10 cm in diameter to a focal spot diameter of about 5 mm (50 % beam diameter). If the whole available skull surface around the brain is utilized, then a window of at least three times larger could be used. In addition, the geometric gain would allow the peak power through the skull to be increased. Acoustic power up to 30- 80 W/cm^2 of the transducer surface area for continuous wave sonication can be generated by ceramic transducers. Higher peak powers could be achieved

with the pulsed sonication used for induction of cavitation. Thus, it is estimated that much higher pressure amplitudes than measured here can be induced in the brain through the skull.

The values measured in connection with the foregoing compare favorably with the 4 MPa that was reported to be the threshold value in vivo muscle at 0.6 MHz and a value of 8.5 MPa at 0.936 MHz in vivo rabbit brain (the threshold at 0.6 MHz would be lower since it has been shown to decrease with frequency). Thus, the results demonstrate that adequate ultrasound transmission through skull can be generated to induce cavitation in the brain.

Our results demonstrate that low frequency beams can be focused through the skull, though, the focus may be shifted from its geometric location. Therefore, it can be helpful to detect the focal spot location in the brain prior to the therapy exposure, e.g., using magnetic resonance imaging to detect the local temperature elevation or cavitation in the brain at exposure conditions that are below the tissue damage threshold. For example, low power test exposures can be delivered through the skull while using MRI to detect the location of the focal spot. Based on the imaging information the location can be corrected to overlap the target volume prior to the therapeutic exposure.

The phase measurements with the arrays support the observation made with the single element transducers showing that at 0.6 MHz 80 % of the phase errors caused by skull are less than 90° and thus, each wave is adding to the pressure wave at the focus. However, at 1.58 MHz over half of the waves had phase shifts that caused the waves to arrive out of phase at the focus. This observation can be explained by the difference in wavelength that is 2.50 mm at 0.6 MHz and 0.95 mm at 1.58 MHz.

The possibility of inducing selective thermal damage at the focus, without damaging the skin or brain surface, may be possible due to the small focal spots achieved with the phase correction. However, the thermal exposures have to be short to reduce blood flow and perfusion effects that are strong in brain tissue. The sharp temperature gradients at the focus transport

more energy away from the focus than in the bone where the beam is wide and the gradients shallow. At 1.58 MHz, full utilization of the skull surface may provide marginally adequate geometric gains to overcome the skull heating problem. However, at lower frequencies especially around 0.5 MHz the focal brain tissue thermal therapy seems feasible although not as likely as utilization of cavitation effects.

The results demonstrate that the effects of the skull to the beam shape can be eliminated using a phased array with proper phase corrections. In the example above, the phase correction was calculated from hydrophone measurements. The same corrections can be made by measuring the skull thickness from CT or MRI scans and then calculating the phase correction required for each array element. The same may be accomplished by sending a short ultrasound pulse from each or selected elements of the of the phased array and then listening for the echo back from the inner surfaces of the skull or other structures in the brain. The effect of the skull on the wave propagation at each location could then be calculated. This can also be done before therapy by mapping the skull effect using ultrasound.

Although good results were achieved with only 60 transducer elements in the phased array, still more and smaller elements may facilitate moving the focal spot inside of the brain. Similarly, at higher frequencies, smaller elements may allow better phase correction further reducing the losses induced by the skull.

Thus, the geometric gain of about 20 that is required to compensate for the losses caused by the skull can be easily achieved by focusing. This is larger than the gain of 10 required to compensate the average losses. This indicates that adequate power for induction of cavitation can be delivered using phased arrays through the skull even at frequencies that are too high with a single element applicator.

In summary, the invention provides methods and apparatus for noninvasive diagnosis and treatment of the brain using cavitational mechanism and pulsed ultrasound. It permits adequate

power transmission through the human skull can be induced to cause tissue damage while keeping the exposures in the overlying tissues below the cavitation threshold.

Those skilled in the art will appreciate that the invention can be applied for purposes of tissue ablation, as well as in other procedures where focussed ultrasound is desired. These include opening the board-brain barrier, activation of therapeutic agents, occlusion of blood vessels, disruption of arteriosclerotic plaques and thrombi, etc. It will also be appreciated that the invention can be applied for treatment of humans, rabbits and other animals. The embodiments discussed above and shown in the drawings are illustrative only. Other embodiments, incorporating substitutions, modifications and other changes therein, fall within the scope of the invention. These include embodiments with transducer arrays of different sizes, shapes and numbers of elements, as well as embodiments with different amplification and driving systems. In view of the foregoing, what I claim is:

INTERNATIONAL SEARCH REPORT

International application No.
PCT/US97/14760

A. CLASSIFICATION OF SUBJECT MATTER

IPC(6) :A61B 17/00
US CL :128/653.1, 660.03; 601/004
According to International Patent Classification (IPC) or to both national classification and IPC

B. FIELDS SEARCHED

Minimum documentation searched (classification system followed by classification symbols)

U.S. : 128/653.1, 660.03; 601/002, 003, 004

Documentation searched other than minimum documentation to the extent that such documents are included in the fields searched

Electronic data base consulted during the international search (name of data base and, where practicable, search terms used)

C. DOCUMENTS CONSIDERED TO BE RELEVANT

Category*	Citation of document, with indication, where appropriate, of the relevant passages	Relevant to claim No.
X	US 5,158,071 A (UMEMURA et al.) 27 October 1992, Abstract, Figs. 1-3, col. 6 lines 14-48 and 63 to col. 7 line 5, and col. 8 lines 1-4 and 66-68.	1-42
X	US 5,524,625 A (OKAZAKI et al.) 11 Junr 1996, Abstract, and Figs. 1-3, 7, 8 and 10-12.	1, 2, 11, 17, 18, 27, 33-42
X, P	US 5,665,054 A (DORY) 09 September 1997, Abstract, Figs. 1-3, col. 5 lines 20-35, col. 6 lines 29-40, col. 7 lines 8-11, and col. 10 lines 32-56.	1-42
X	US 5,316,000 A (CHAPELON et al.) 31 May 1994, Abstract, Figs. 1, 2 and 5.	1-5, 11, 17-21, 27, 33-40

[X] Further documents are listed in the continuation of Box C. [ ] See patent family annex.

*	Special categories of cited documents:	"T"	later document published after the international filing date or priority date and not in conflict with the application but cited to understand the principle or theory underlying the invention
"A"	document defining the general state of the art which is not considered to be of particular relevance	"X"	document of particular relevance; the claimed invention cannot be considered novel or cannot be considered to involve an inventive step when the document is taken alone
"E"	earlier document published on or after the international filing date	"Y"	document of particular relevance; the claimed invention cannot be considered to involve an inventive step when the document is combined with one or more other such documents, such combination being obvious to a person skilled in the art
"L"	document which may throw doubts on priority claim(s) or which is cited to establish the publication date of another citation or other special reason (as specified)	"&"	document member of the same patent family
"O"	document referring to an oral disclosure, use, exhibition or other means		
"P"	document published prior to the international filing date but later than the priority date claimed		

Date of the actual completion of the international search
14 OCTOBER 1997

Date of mailing of the international search report
12 NOV 1997

Name and mailing address of the ISA/US
Commissioner of Patents and Trademarks
Box PCT
Washington, D.C. 20231
Facsimile No. (703) 305-3230

Authorized officer
SHAWNA J. SHAW
Telephone No. (703) 308-2985

Form PCT/ISA/210 (second sheet)(July 1992)*

INTERNATIONAL SEARCH REPORT

International application No.
PCT/US97/14760

C (Continuation). DOCUMENTS CONSIDERED TO BE RELEVANT

Category*	Citation of document, with indication, where appropriate, of the relevant passages	Relevant to claim No.
X, P	US 5,643,179 A (FUJIMOTO) 01 July 1997, Abstract, Figs. 1-3 and 9, and claims 1-4 and 11-14.	1-42
A	US 5,431,621 A (DORY) 11 Jul y1995, Abstract, Figs. 1 and 3.	1-42
A, P	US 5,656,015 A (YOUNG) 12 August 1997, Abstract, Figs. 1 and 4.	1-42
A, P	US 5,590,657 A (CAIN et al.) 07 January 1997, Abstract, and Figs. 1-3.	1-42

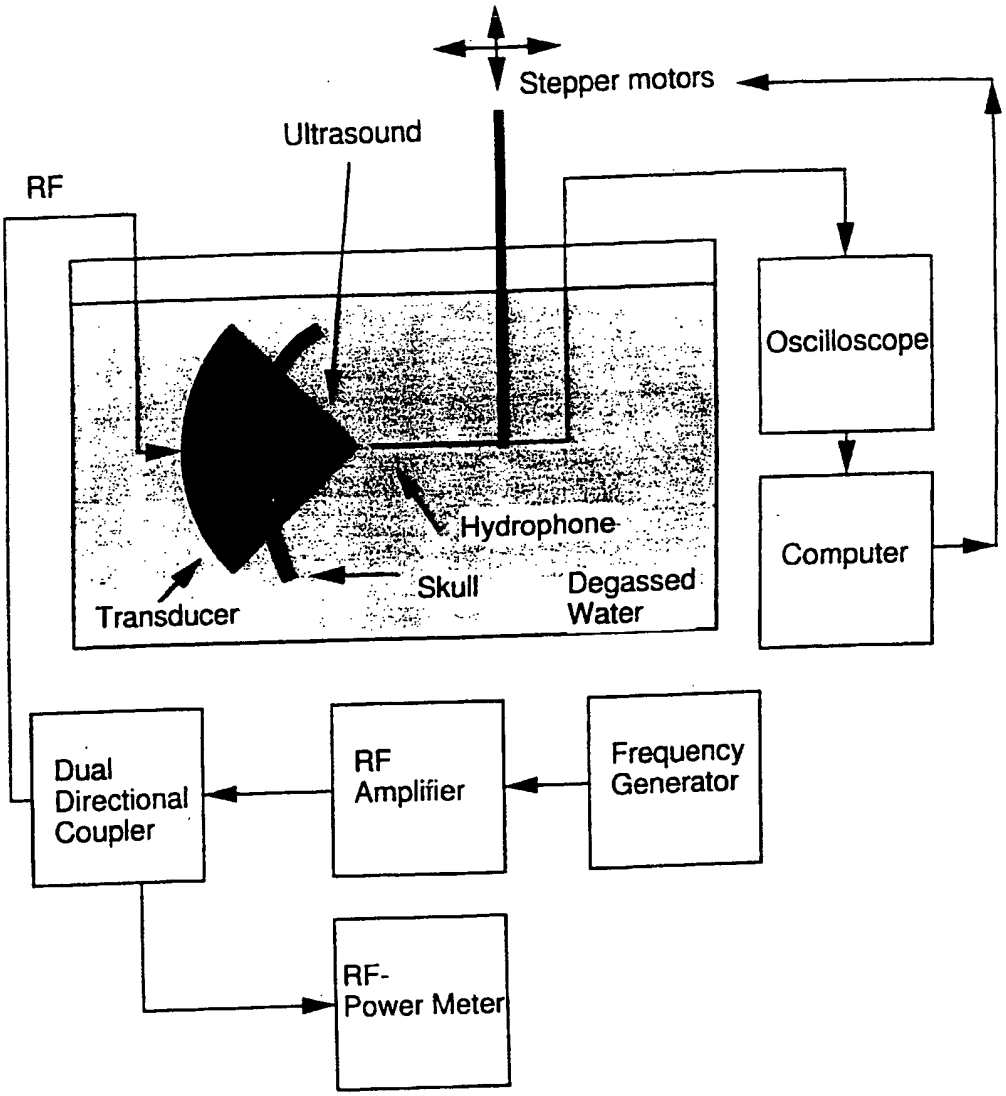
Stepper motors
Ultrasound
RF
Oscilloscope
Hydrophone
Computer
Skull
Degassed Water
Transducer
Dual Directional Coupler
RF Amplifier
Frequency Generator
RF- Power Meter

Figure 1

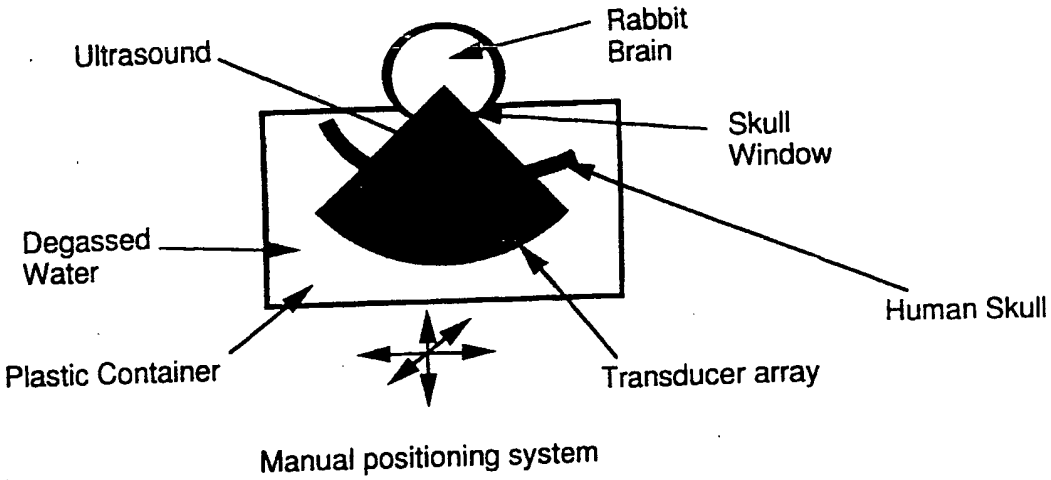
Ultrasound
Rabbit Brain
Skull Window
Degassed Water
Human Skull
Plastic Container
Transducer array
Manual positioning system

Figure 2.

1.58 MHz

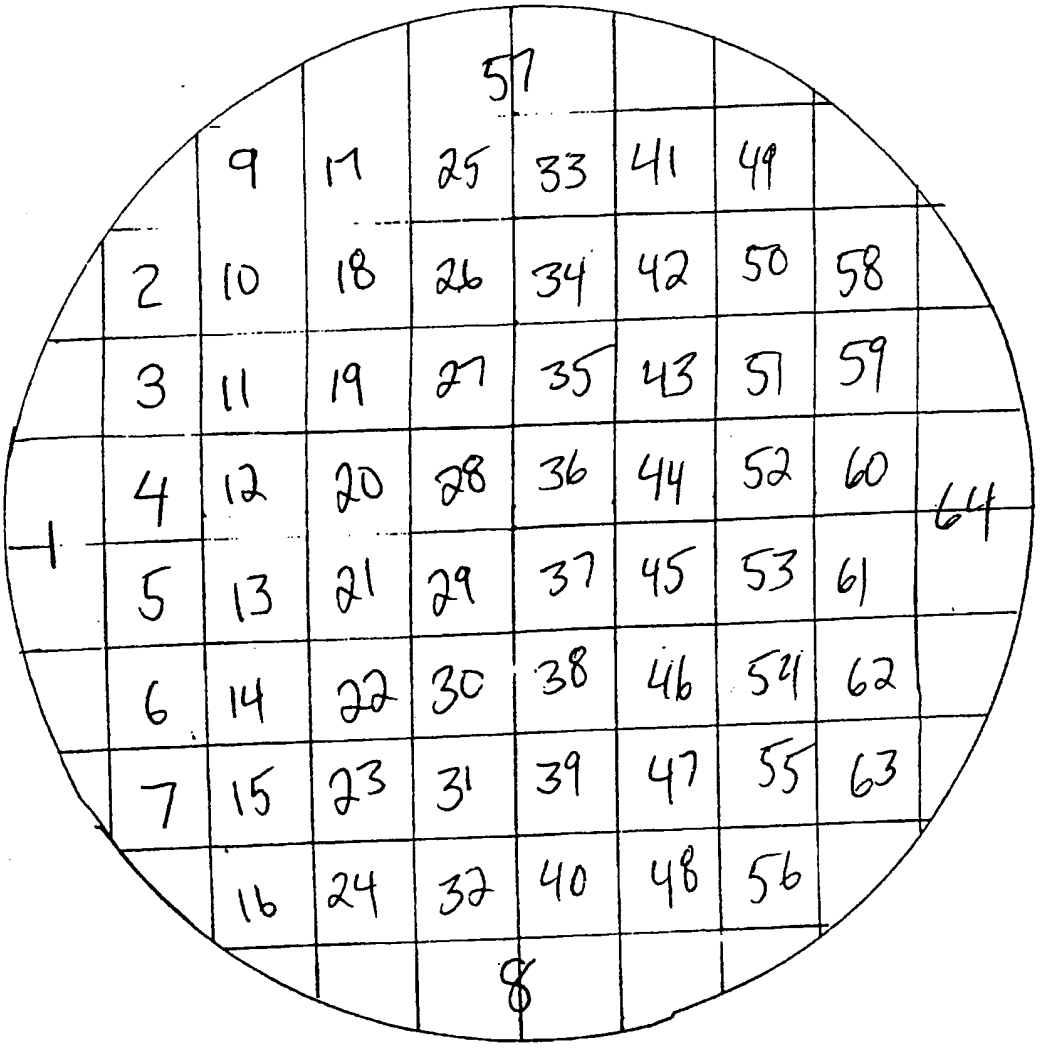

Back of Tx r

Figure 3

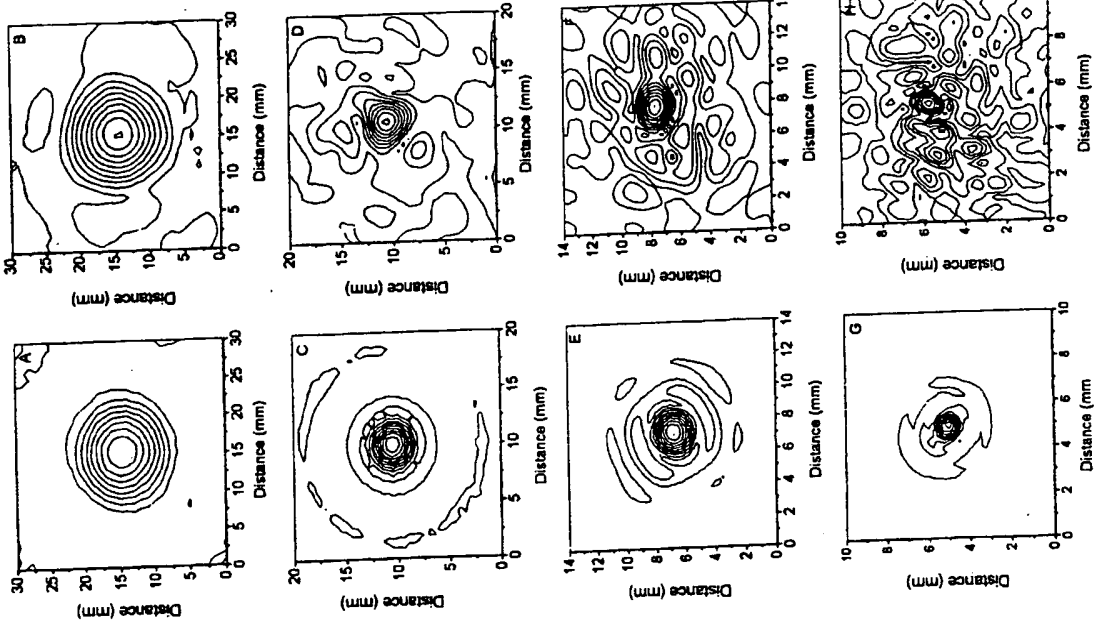

Fig. 4A Fig. 4B Fig. 4C Fig. 4D Fig. 4E Fig. 4F Fig. 4G Fig. 4H

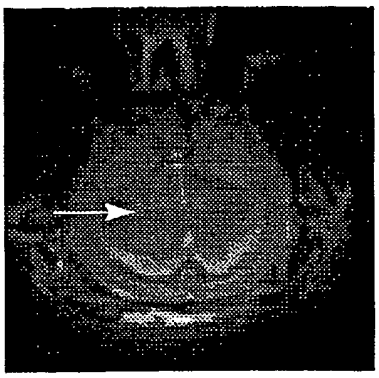

Figure 5A

Figure 5B

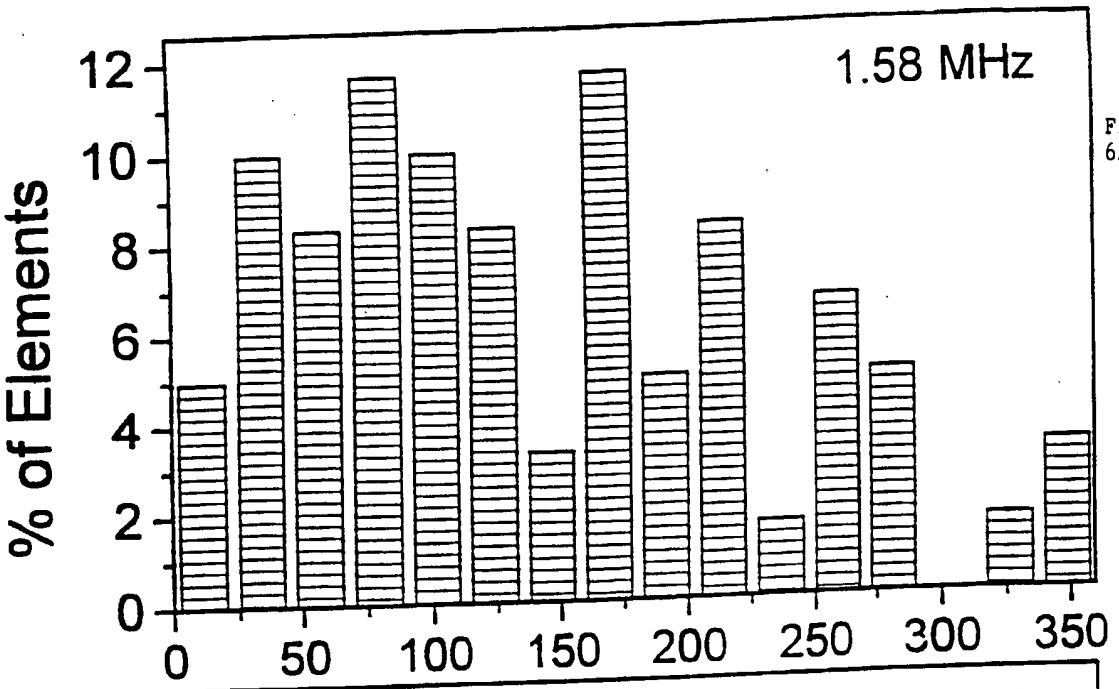
1.58 MHz
% of Elements
0
2
4
6
8
10
12
0
50
100
150
200
250
300
350

Fig. 6A

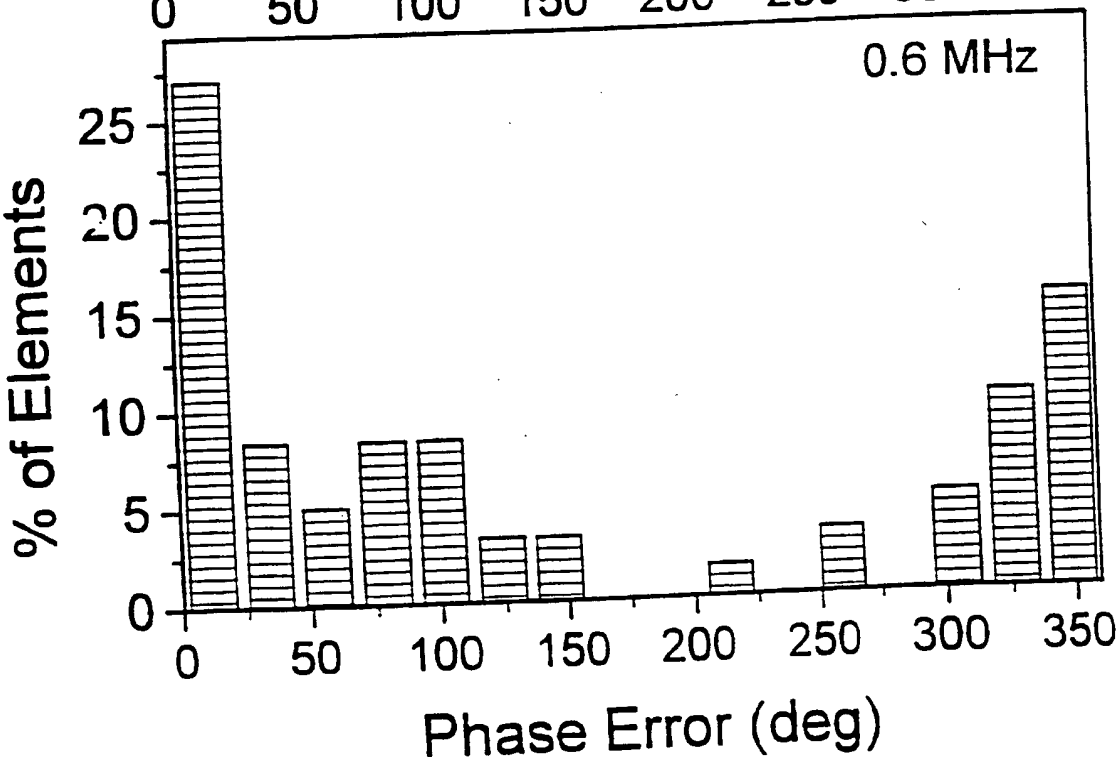
0.6 MHz
% of Elements
0
5
10
15
20
25
0
50
100
150
200
250
300
350
Phase Error (deg)

Fig. 6B

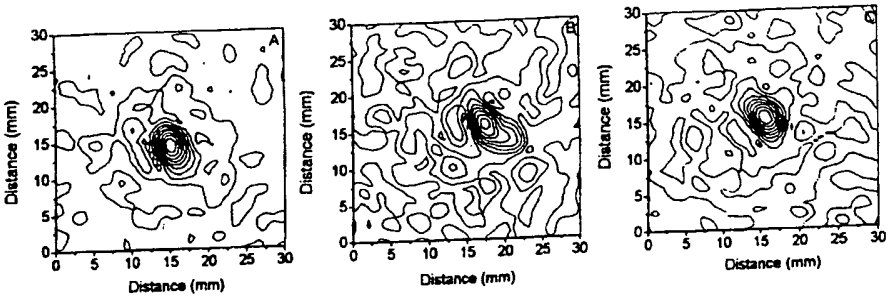

Fig. 7A

Fig. 7B

Fig. 7C

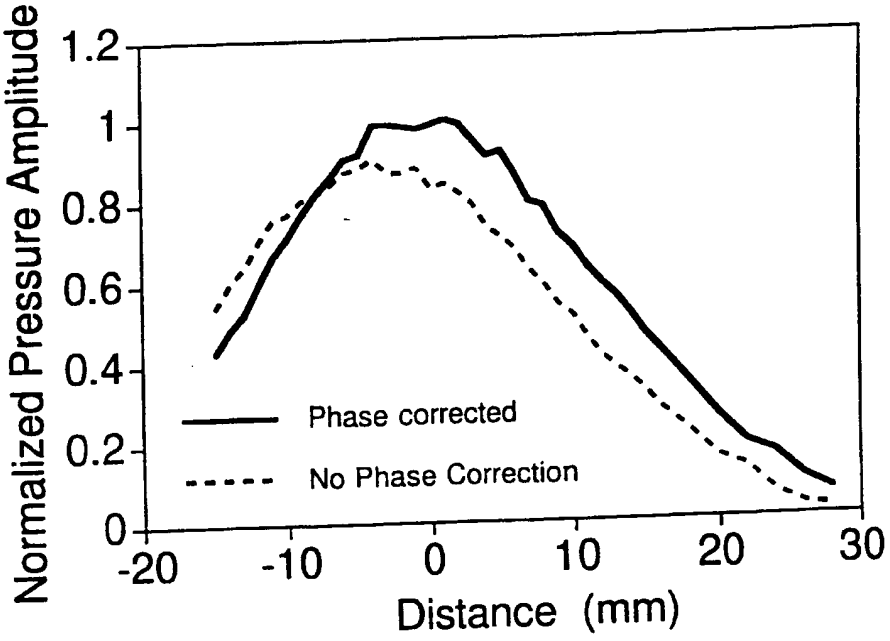
Normalized Pressure Amplitude
1.2
1
0.8
0.6
0.4
0.2
0
-20
-10
0
10
20
30
Distance (mm)
Phase corrected
No Phase Correction

Figure 8

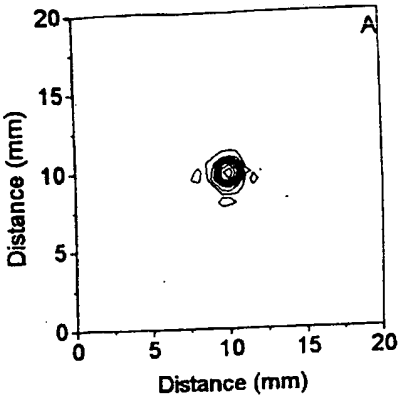

Fig. 9A

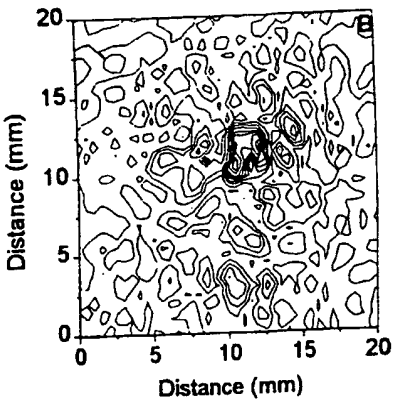

Fig. 9B

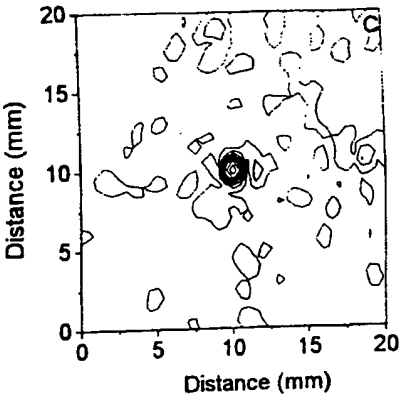

Fig. 9C

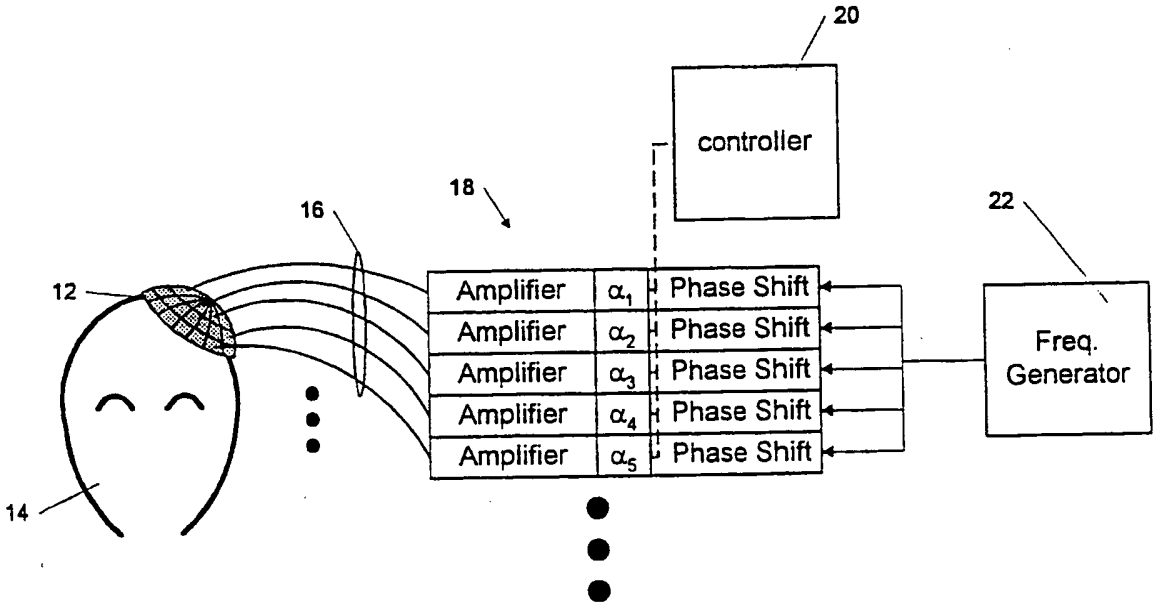
20
controller
18
16
22
12
Amplifier
α_1
Phase Shift
Amplifier
α_2
Phase Shift
Amplifier
α_3
Phase Shift
Amplifier
α_4
Phase Shift
Amplifier
α_5
Phase Shift
Freq.
Generator
14

Figure 10

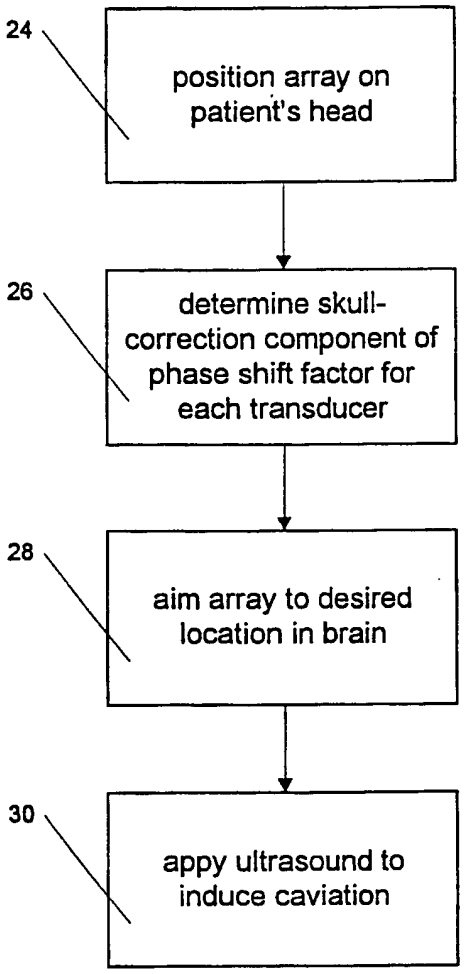
24
position array on patient's head
26
determine skull-correction component of phase shift factor for each transducer
28
aim array to desired location in brain
30
appy ultrasound to induce caviation

Figure 11

Attachment I

to Patent Application for

Methods and Apparatus for Delivery of Noninvasive Ultrasound Brain Therapy Through Intact Skull

---

Buchanan *et al*, "The Design and Evaluation of an Intracavitary Ultrasound Phased Array for Hyperthermia," IEEE Trans. Biomed. Eng., v. 41, pp. 1178 - 1187 (1994)

Design and Experimental Evaluation of an Intracavitary Ultrasound Phased Array System for Hyperthermia

Mark T. Buchanan and Kullervo Hynynen

Abstract— For evaluating the feasibility of treating prostate cancer, a 64-element linear ultrasound phased array applicator for intracavitary hyperthermia was designed and constructed. A 64-channel ultrasound driving system including amplifiers, phase shifters, and RF power meters was also developed to drive the array. The design of the array and driving equipment are presented, as are the results of acoustical field measurements and *in vitro* perfused phantom studies performed with the array. Several techniques for heating realistically sized tumor volumes were also investigated, including single focus scanning and two techniques for producing multiple stationary foci. The results show that the operation of the array correlated closely with the theoretical model. When producing a single stationary focus, the array was able to increase tissue temperature by 12°C *in vitro* in perfused phantom. With some minor improvements in array design, intracavitary phased arrays could be evaluated in a clinical environment.

I. Introduction

INTRACAVITARY ultrasound arrays offer an attractive means of inducing local hyperthermia in deep-seated tumors located near body cavities. By locating the radiators as close as possible to the treatment site, problems frequently encountered with external techniques, such as blockage of the acoustic window by bone or gas, or simply the inability to attain adequate energy penetration, can be avoided. Early results using multielement, nonfocused arrays of half-cylinder transducers operating at 1.6 MHz suggest that such arrays can be clinically useful in the treatment of prostate cancer [1].

The proximity of the prostate to the rectum wall makes it a good candidate for heating using intracavitary ultrasound radiators. Since the prostate is located very near the anus and only millimeters away from the rectum wall, an applicator can be easily located close to the prostate. The prostate is one of the most easily accessible tumor sites, and one that affects a large enough population of patients to be potentially clinically useful. As such, most of the experiments were conducted with the goal of heating the prostate in mind.

While the nonfocused arrays have shown considerable potential in heating the prostate, they have two primary limitations: the depth to which they can effectively heat, and their limited ability to control the power deposition fields [2], [3]. Both deeper penetration and increased control over the power deposition pattern can be achieved using linear phased arrays. Since phased arrays can focus their radiated energy, they theoretically could heat tissues to therapeutic temperatures deeper than nonfocused arrays. The ultrasound power deposition pattern can be electronically tailored as necessary to produce therapeutic temperatures within a desired volume. In areas where heating would be undesirable, the phased array could take advantage of destructive interference to minimize power deposition at those locations. The ease by which the power deposition pattern can be electronically altered in real time provides a means for the compensating for varying physiological parameters, patient positioning, and for minimizing patient discomfort.

Several types of ultrasound phased arrays have been proposed or built for hyperthermic purposes. These include Umemura and Cain's sector-vortex and concentric ring applicators [4], [5], the cylindrical section applicator developed by Ebbini *et al.* [6], [7], as well as the tapered array developed by Benkeser *et al.* [8]. Each of these arrays is composed of anywhere from 16 to 64 individual elements and operates at frequencies between 500 kHz and 750 kHz. While these arrays show significant potential, they are meant to be used in external applications and therefore are unsuitable for intracavitary use in their reported configurations.

Previously, a theoretical study on the feasibility of intracavitary phased arrays using half-cylinder elements had been done by Diederich and Hynynen [3]. Based on many acoustical and thermal simulations, it was concluded that a practical array would be composed of 30 half-cylinder elements with 2.5 mm center-to-center element spacing operating at 500 kHz. The study predicted that the grating lobes formed with this array could be negated by using surface cooling. One of the major considerations in specifying this design was not the performance of the array, but the apparent high cost of the amplifiers necessary to drive the system. The desire to minimize the number of amplifiers led to the specification of a 30-element array.

Initial array designs were based on some recommendations from the theoretical study and expanded upon in an attempt to construct a practical intracavitary phased array. It became apparent that more than 30 amplifiers would be necessary for

Manuscript received November 17, 1992; revised August 9, 1994. This work was supported by grant number RO1 CA 46939 from the National Cancer Institute.

The authors are with the Department of Radiology, Division of MRI, Brigham and Women's Hospital, Harvard Medical School, Boston, MA 02115 USA.

IEEE Log Number 9406164.

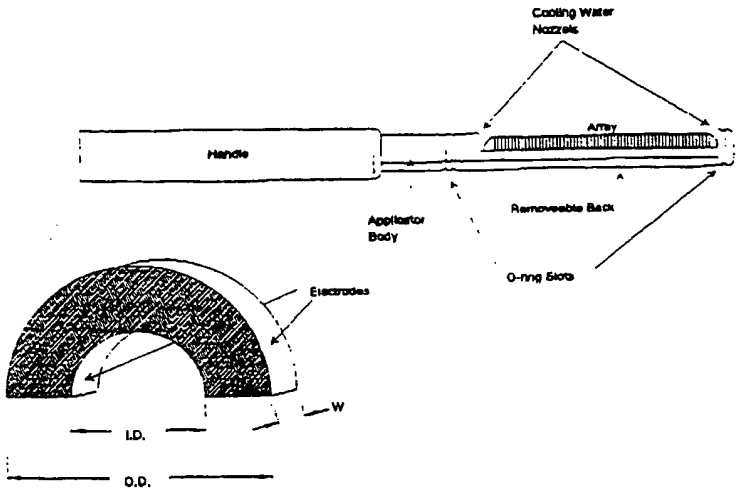

Fig. 1. The 64-element array and a single element showing the geometry of the array. The array was mounted to a brass shell 19 mm in diameter. The back of the applicator was removable so that wires could be connected to the inner electrodes.

a useful array. This led to the development of the 64-channel driving system to overcome the limitations imposed by the number of amplifiers. This allowed for the evolution of a 64-channel phased array with 1.73 mm center-to-center spacing and a total array length of 110.5 mm operating at 500 kHz.

II. Materials and Methods

A. Array Construction

A 64-element array was constructed using half-cylinder transducers operating in their resonant radial mode at 500 kHz. The array was made by slicing washer-shaped elements with a diamond wire saw (Laser Technologies, North Hollywood, CA) from 15 mm O.D. by 30-mm long cylinders of PZT-4 material (EDO, Salt Lake City, UT) with silver electrodes plated on both the inner and outer wall surfaces. The transducer slices were glued together using a silicone adhesive (Dow Corning, Midland, MI) with 0.17-mm thick silicon rubber spacers (SPC Technology, Chicago, IL) between each element (producing a dead space of 0.23 mm between elements). The stack of elements was then cut in half along the axis of the cylinder and the two half-cylinder sections glued together to form the full array. The array was bonded to a brass shell to form the complete applicator, as shown in Fig. 1. Wires were soldered to the inside wall of each array element that extended the length of the shell to the handle where they were each connected to a 2-m RG-178 coaxial cable. The electrodes on the outer surface of the array were electrically connected by single wires embedded in beads of silver epoxy (Chomerics, Woburn, MA) running along both edges of the array.

B. Driving Hardware

One of the primary disadvantages of phased arrays is the increased complexity of the driving equipment. Due to a lack of commercially available equipment to drive the array, a 64-channel amplifier system was developed. This system is composed of phase shifters/duty cycle controllers, amplifiers, RF power meters, and impedance matching networks (see block diagram in Fig. 2) and is controlled by an IBM PC compatible computer via a digital I/O interface.

The amplifiers are based on a switching MOSFET design and are designed around International Rectifier's IR2110 dual MOSFET driver. Each of the amplifiers is capable of delivering up to 16 W of RF power at 500 kHz into a 50-W load from each channel or a total output power of about 850 W. The amplifiers convert digital logic input signals into high power sine waves while preserving the phase of the input signal. The amplitude of the output signal is controlled by two methods. All of the amplifier outputs can be controlled simultaneously by adjusting the output voltage on a 1000 W DC supply, or the output of each channel can be individually controlled by varying the duty cycle of the input signal. The result of reducing the duty cycle of the input signal (the duty cycle is the percent of "on" time of the input signal per clock cycle) is a corresponding decrease in the amplitude of the output signal.

Since the amplifiers require digital input signals, the phase shifting and duty-cycle control is implemented using digital counters [10], [11]. These circuits provide 22.5° phase shift resolution from 0–360°, and 16 steps of duty cycle (amplitude) that allows the output to vary from 0–100% of the output power, as allowed by the voltage from the DC supply. While the phase shift resolution may seem somewhat limited, studies have shown that it is sufficient for the uses described here [11], [12].

The actual RF output power from each channel is monitored by power meters that measure both the forward and reflected RF power [13]. The power meters, which were also designed

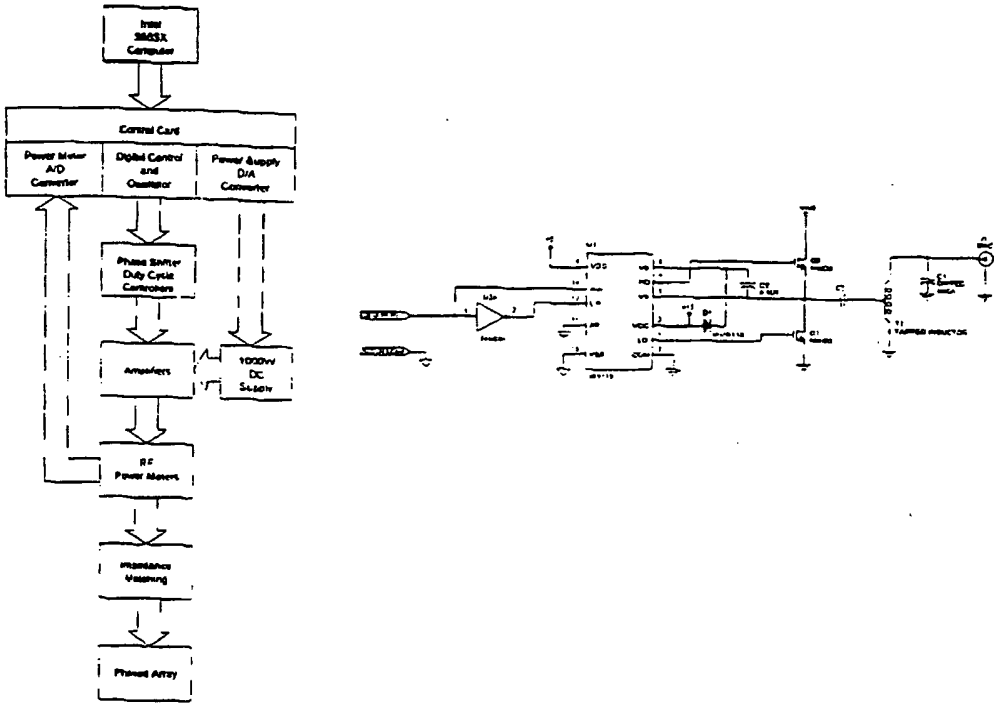

(a) (b)

Fig 2 (a) Block diagram of the phased array driving system. (b) A simplified schematic of the switching amplifiers

TABLE I
NOMENCLATURE AND DEFAULT VALUES USED IN THE NUMERICAL STUDIES

f	frequency	500 kHz
c	velocity	5 Np m^{-1}
a	Radius of simple source	$\lambda/32$
λ	wavelength	3.0 mm

and constructed in house, allow for verification of the output power on each of the amplifier channels, and allow for the monitoring of the outputs so that possibly dangerous fault conditions do not occur. By monitoring the amount of reflected power, changes in the electrical matching and the array operation can be easily monitored so that peak array performance can be maintained.

Finally, to maximize power transfer between the amplifiers and array elements, a simple LC impedance matching network was used on each channel between the power meters and the array. This not only maximizes power transfer, but ensures greater uniformity in the acoustical output signals for a given excitation phase and amplitude verified experimentally by a needle hydrophone. Without electrical matching, the phase shift and amplitude distortion caused by the impedance differences between elements in the array would have to be characterized using a hydrophone and the results used to compensate the excitation signals.

C Acoustic Modeling

The 3-D ultrasound modeling program used was originally developed by Diederich and Hynynen [3] and is only briefly introduced here. The routine models N cylindrical radiators of finite length, radius and separation as each of the ultrasound transducers in the array, and assumes a target media having similar acoustical properties as tissue (Table I). The routine models the surface of each of the cylindrical elements as an evenly spaced grid of simple hemispherical sources and uses Huygens principle to sum the contributions of each source at each point in the field. All of the simulations were done with the sources spaced on a $\lambda/32$ grid.

The acoustical pressure field was calculated in the z-plane using

$$P(z,r) = \left| \sum_{j=-\frac{n_\theta}{2}}^{\frac{n_\theta}{2}} \sum_{i=1}^{n_z} P_s(r_{ij}) \right| \quad (1)$$

where

$$P_s(r) = \frac{P_{so} r_o}{r} e^{j(2\pi f - 2\pi \frac{r}{\lambda} - \phi) - \alpha r} \quad (2)$$

and n_z is the number of sources in the z-direction, n_θ is the number of sources in the theta direction. P_s is the pressure from a single source (Pa), P_{so} is the pressure amplitude at the surface of the source (Pa), r_o is the radius of the source (m), r is the radial distance from the center of the source (m), λ is the wavelength (m), ϕ is the phase of the excitation signal (rad), f is the operating frequency (Hz), and α is the attenuation coefficient (Np/m).

D. Focusing Techniques

The single focus case is the simplest form of focusing that can be done with a phased array. The single focus is produced by setting the phases of the driving signals so that constructive interference occurs at the desired focal position. The phase of each of the driving signals for an array with N elements can be calculated from the differences in the path lengths d_i between each array element and the focal position by

$$\varphi_i = 2\pi \frac{\Delta d_i}{\lambda} + 2\pi m \quad (3)$$

where f_i is the phase (radians) of the i^{th} element, λ is the wavelength (m), $i = 1, 2, \ldots, N$ and $m = 0, 1, 2, \ldots$. The size of the focus produced with this technique is usually too small to heat an entire tumor volume, and therefore other techniques must be used to heat larger volumes.

To heat larger volumes, two techniques were investigated: single-focus scanning and multiple focusing. The single focus scanning routine simply stepped a single focus back and forth along a predetermined length of the array. The focal depth was kept constant while the focus was stepped every 300 ms to the next position in the scan. Delivered power was maximal at the edges of the scan but was reduced to 64% of maximum power at the center of the scan to flatten the temperature distribution in the perfused phantom experiments (the power distribution was experimentally determined).

The other technique, multiple focusing, simultaneously produces more than one focus within the target volume. The driving signals necessary to produce multiple foci were calculated using two techniques: split focusing and the pseudo-inverse. To create multiple foci with the split focusing technique, the array was divided into subarrays, each of which produce a single focus in the same manner as previously described. The pseudo-inverse method, developed by Ebbini and Cain [15], uses a series of control points that represent the magnitude of the ultrasound field at given points. A brief summary of Ebbini and Cain's technique follows.

The technique solves the Rayleigh-Sommerfeld integral for an array with N elements, and a field of M control points $p(r)$

$$p(r_m) = \frac{j\rho ck}{2\pi} \sum_{n=1}^{N} u_n \sum_{S'_n} \frac{e^{-jk|r_m - r'_n|}}{|r_m - r'_n|} dS'_n \quad (4)$$

where ρ is the density of the propagation medium, c is the speed of sound in the medium, k is the wavenumber, S' is the surface of the source, u_n is the particle velocity normal to the surface of the source, and $r_m - r_n$ is the distance between a control point (r_m) and the surface of a source (r_n). $m = 1, 2, \ldots, M$, and $n = 1, 2, \ldots, N$.

To simplify programming of this algorithm, (4) can be described by

$$Hu = p \quad (5)$$

where u is the excitation vector, p is the complex pressure at the control points, and H is the remainder of (4). For intracavitary hyperthermia uses, the number of elements in the array (N) is always greater than the number of control points (M). This leads to an underdetermined system of equations with an infinite number of solutions. The minimum norm solution ($\hat{u}$) can be determined by using a least squares approximation of (5)

$$\hat{u} = H^{*t}(HH^{*t})^{-1}p \quad (6)$$

where H^{*t} is the complex conjugate of H. With this technique, all of the array elements contribute to all of the foci, unlike the split focusing technique where each element contributes to only one focus.

III. Experimental Techniques

A. Acoustical Efficiency Measurements

The acoustical output of the cylindrical transducer elements was measured using a radiation force technique [16]. The array was placed in a brass cone with 45° sides to reflect the radially emitted ultrasound fields down into the acoustical absorber [17]. The force on the absorber was measured using a Metler AE 160 (Hightstown, NJ) microbalance, while the RF power was measured using a Hewlett Packard 438A RF power meter and a Werlatone C2625 (Brewster, NY) dual directional coupler. The efficiency was calculated as the ratio of the acoustical power to the RF electrical input power.

B. Ultrasound Field Measurements

The ultrasound fields were mapped in a tank of degassed, deionized water by mechanically scanning a thermocouple embedded in a small (2-mm diameter) plastic sphere. The thermocouple was positioned by a three-axis computer controlled scanning table. The applicator was mounted on a rotational device that allowed measurements to be made in a radial arc around the array by rotating the array. Measurements were made on a 1 × 1 mm grid with the recorded data being the average of three consecutive measurements.

C. In Vitro Kidney Experiments

Alcohol fixed canine kidneys were used as phantoms for studying the heating characteristics of the array. The kidneys had previously been prepared as described by Holmes *et al.* [18], and were rehydrated prior to use. The experiments were conducted at room temperature using degassed, deionized water as the perfusate. A metering pump (Fluid-Metering Inc., RHICKC, Oyster Bay, NY) connected to the renal artery circulated water through the kidney while the renal vein was allowed to drain into the tank. The kidney was held in place by gently sandwiching it between two PVC membranes mounted to a Plexiglas frame. The applicator was firmly clamped to the frame to maintain a fixed distance between the surfaces of the kidney and array. Fig. 3 shows a diagram of the experimental setup.

Temperatures were measured in the kidney using either seven sensor probes sutured in place perpendicular to the array through the focal region, or by one or two single sensor thermocouples pulled along a path parallel to the array. In experiments conducted with the multiple sensor probes, the kidney was exposed to ultrasound for a total of 10 min with temperature measurements occurring every 30 s. During each temperature measurement, power to the array was disrupted for approximately four seconds (one second prior to the first reading, and up to three seconds to read all of the thermocouples). Since this technique does not give very fine spatial detail of the temperature distributions, the pull-back technique was more frequently used.

The pull-back experiments were conducted by pulling one or two single uncoated thermocouples (0.05-mm wire) by a computer controlled stepper motor along a track parallel to the array through the kidney tissue. The temperatures were measured every 1 mm and the average of three readings was recorded. Prior to each of the experiments, a baseline temperature was established along the path of the thermocouples. The kidney was exposed to ultrasound for 20 min to allow the temperatures to reach steady-state before the temperature profiles were measured. The difference between the baseline and final measurement was used to calculate the temperature rise. The kidney was allowed to cool to room temperature (typically, 30 min) before to the next experiment was started.

The thermocouples were mainly located in the medulla of the kidney. The steady-state temperatures in the medulla have been shown to be a strong function of the flow into the kidney [19]. The flow values were kept relatively low in order to simulate the perfusion in the prostate [20], [21].

IV. Results

A. Acoustical Efficiency Measurements

The acoustical efficiency of the 500-kHz PZT-4 transducer material was measured for a full cylinder, 30 mm long, and for two half-cylinder arrays with 2.5 mm and 1.8-mm center-to-center element spacing (2.2 mm and 1.5 mm element widths) with total array lengths of 24.7 mm and 28.5 mm, respectively. Small arrays were tested so that the resulting field would be collimated, unlike a single array element

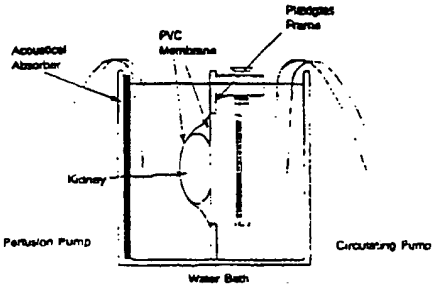

Fig. 3. Diagram of the *in vitro* kidney experimental setup

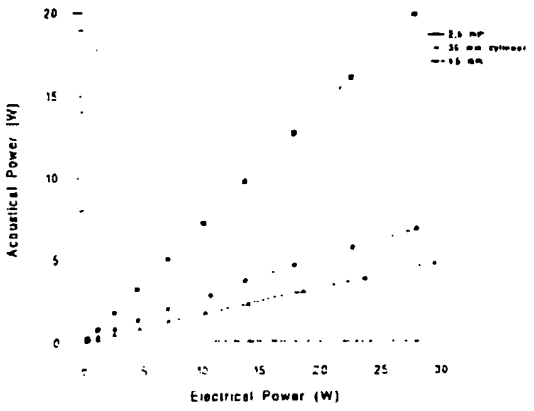

Fig. 4. Acoustical output power as a function of electrical input power for a single 30-mm, full cylinder element, and arrays made up of 16 2.2-mm and 1.5-mm elements with a 0.3-mm insulator between elements.

(width < wavelength), which would produce nearly spherical wavefronts. The collimation is necessary to assure the waves reflected by the reflector are normally incident to the surface of the absorber.

The results of these experiments are shown in Fig. 4. None of the arrays exhibited very high efficiencies despite the low operating frequency. Though not shown here, some results were verified using calorimetric techniques. While the 30-mm long full cylinder element had an efficiency of 71%, the arrays exhibited efficiencies of 27% and 17% for the 2.2-mm and 1.5-mm arrays, respectively. These efficiencies indicate that about 80% of the electrical power delivered to the 1.5-mm wide elements used in the phased arrays is lost either as heat in the transducer or in the electrical matching and transmission lines between the amplifier and the array.

B. Ultrasound Field Measurements

The effects of element spacing were studied by measuring the ultrasound field distributions produced by two 16-element arrays with 1.8-mm and 2.5-mm center-to-center element spacing. Fig. 5(a) and (b) shows the acoustical field plots made in a plane parallel to the array and normal to the surface of

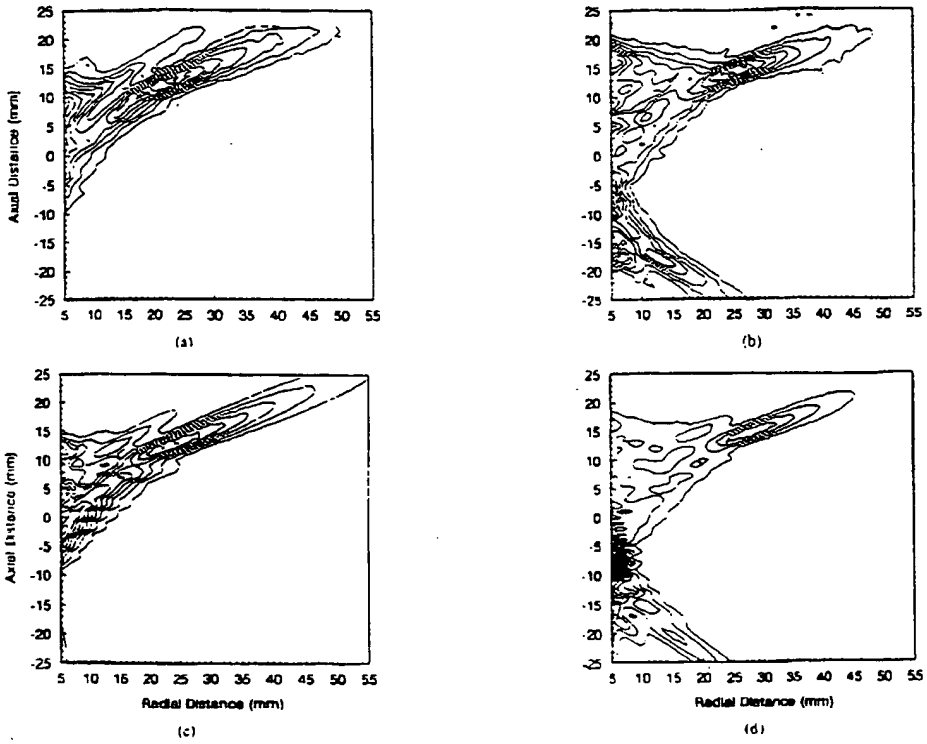

Fig. 5. Field plots in water of two 16-element arrays with 1.8-mm (a) and 2.5-mm (b) element center-to-center spacing and their corresponding simulation results (c) and (d)). Both arrays were focused 30 mm from the array surface and 15 mm from the central axis.

the half cylinder elements for two 16-element arrays with 1.8-mm and 2.5-mm element spacing along with their respective simulated fields (Fig. 5(c) and (d)). Both arrays were focused 30 mm from the array surface and 15 mm above the central axis of the array. The most significant effect illustrated here is the generation of the grating lobe by the 16-element array with 2.5-mm center-to-center element spacing (Fig. 5(b) and (d)). Since such a large grating lobe not only reduces the power of the focus but also could cause heating in unwanted areas, arrays must be designed to minimize grating lobe formation. The array with 1.8-mm center-to-center spacing produced much better field distributions than the array with 2.5-mm center-to-center spacing. Therefore, in order to have center-to-center spacing 1.8 mm or smaller, 1.5-mm wide elements were used in the final array design and the dead space between elements was reduced to 0.23 mm.

The complete measured and simulated plots of the ultrasound field produced by the 64-element array with 1.73-mm element spacing are shown in Fig. 6(a) and (b), respectively. The array was focused 40 mm deep, and 30 mm from the central axis. Note that only a small grating lobe is produced by this array even though it is focused a substantial distance from its central axis. In fact, this array is capable of focusing to about 35° from the central axis of the array without producing significant grating lobes.

So far, all of the acoustical field measurements presented have been in a plane parallel to the length of the array and normal to the surface of the array. Ideally, the acoustical field would taper off toward the edges of the array but be more or less uniform around the arc of the array. Unfortunately, this ideal does not match reality, as can be seen in Fig. 7. The acoustic field was measured as a function of rotation angle along a line by fixing the position of the thermocouple in the focal region and rotating the array about its axis. The acoustical intensity is not at all uniform and, in fact, varies as much as 50% before tapering off at the edges. All of the 2-D acoustical field plots shown here were made at the 0° rotation angle where the intensity is only about 50% of the peak. Measurements made, but not shown here, show that this fluctuation in pressure amplitude due to the rotation angle only alters the peak intensity and does not effect the overall shape of the acoustic field.

Fig. 8(a) and (b) shows the acoustical field plots produced using the two multiple focus techniques: pseudo-inverse and split focusing. Below them, in Fig. 8(c) and (d), are their respective simulation results. Both techniques were used to synthesize foci 40 mm from the array surface and 10 mm on either side of the central axis of the array (20 mm apart) using the 64-element array. Notice that the pseudo-inverse technique produces sharper foci than those produced by the

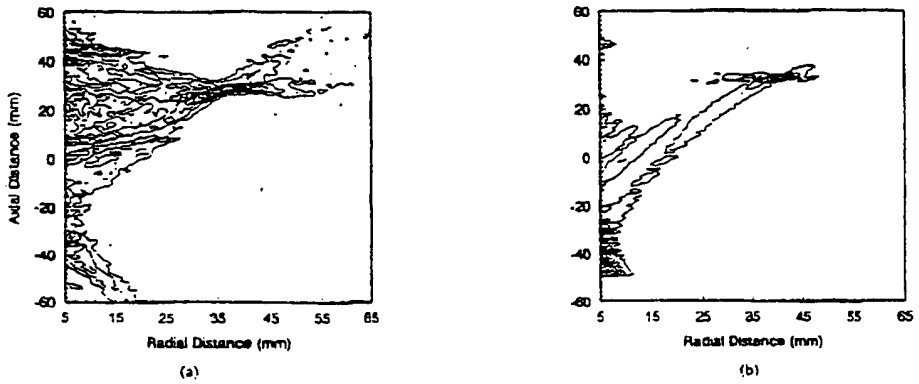

Fig. 6. Field plot of the 64-element array (a) along with the simulation results (b) for focus 40 mm from the surface of the array and 25 mm off its central axis.

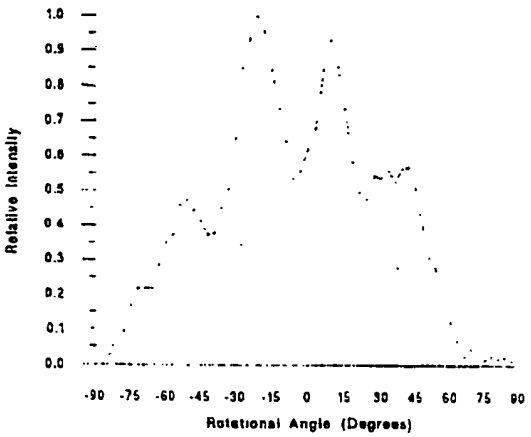

Fig. 7. Single dimensional radial field plot made within the focus as a function of the angle of rotation of the array. The center of the array arc is defined as the zero point.

split focusing method. This occurs because the pseudo-inverse technique utilizes the entire length of the array allowing it to produce sharper foci than the split focusing technique which, since it divides the array into two subarrays, effectively uses array lengths only half as long as the actual length of the array.

C. In Vitro Kidney Experiments

Fig. 9(a) shows the temperature rise versus time along a fixed seven-sensor thermocouple probe located perpendicular to the array. The distances marked denote the distance of the thermocouple from the edge of the kidney nearest to the array. The array, with 32 active elements, was focused along its central axis and 10 mm into the kidney. (Thirty-two active elements were used since the array length in this configuration could adequately cover the kidney.) The kidney was perfused at a rate of 2.9 kg m^{-3} s^{-1}. Note that the kidney is only 35 mm thick and thus, the temperatures close to the surfaces of the kidney are dominated by cooling caused by the circulating water in the water bath. All of the following results were obtained in the center of the kidney where the focus was located and the surface effects were smallest. The temperature rises achieved in the middle of the kidney indicate that therapeutic temperatures can be achieved with a stationary single focus at realistic perfusion levels. Typical cross-section profiles measured in the middle of the kidney with the pull-back technique for a center focus and 15 mm on either side are shown in Fig. 9(b).

The three different techniques for heating larger volumes: pseudo-inverse, split focusing, and scanned single foci are compared in Fig. 10(a) and (b). The two multiple focusing techniques were used to produce foci 40 mm from the surface of the array and 10 mm on either side of the array's central axis, while the scanning routine produced a series of single foci 40 mm from the array surface with a total span of 20 mm. The thermocouples were located 8 mm and 15 mm from the surface of the kidney nearest to the array (35 mm and 42 mm from the surface of the array). The scanning technique produced a narrower profile than the two multiple focusing techniques and the distribution lacks the temperature drop between foci. The two multiple focusing techniques produce virtually identical profiles, although the pseudo-inverse technique does not produce as large of a temperature rise on the deeper thermocouple (beyond the focus) as does the split focusing technique. This is caused by the increased sharpness of the foci produced by the pseudo-inverse technique, as previously explained.

V. Discussion and Summary

An intracavitary ultrasound phased array composed of half-cylinder transducer elements has been constructed for inducing hyperthermia in the prostate via the rectum. A 64-channel amplifier system has also been designed and constructed to drive the phased array. As was shown by the acoustical field plots, the array is capable of producing focused fields as well as fields containing more than one focus. The array is currently capable of producing a 12°C temperature rise in a perfused phantom using a stationary focus, and smaller temperature

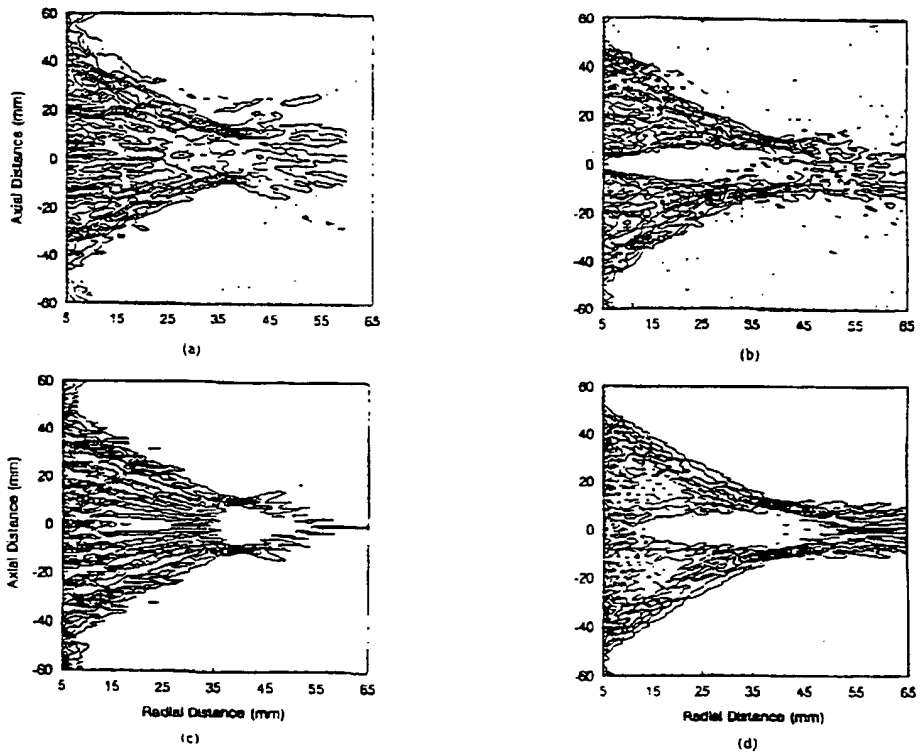

Fig. 8. Acoustical field plots produced using the pseudo-inverse (a) and split focusing (b) techniques and the related simulated results ((c) and (d)). The foci were produced 40 mm deep, and 10 mm on either side of the central axis of the array.

increases were achieved in larger volumes by scanning the focus or by creating multiple stationary foci. This was achieved with flows to the kidney that should simulate the relatively low perfusion in prostate [20], [21].

What has yet to be conclusively shown is such an array's ability to heat tissues to therapeutic temperatures in a regular and predictable manner. The peak temperatures achieved within the perfused phantoms tended to vary considerably from experiment to experiment, making direct comparisons between the absolute temperature profiles difficult. Therefore, the temperature profiles that compare various focusing techniques were normalized to better illustrate the overall differences in the shape of the temperature profiles. The fluctuations in temperature were caused by a variety of problems, including morphological differences in kidneys and the location of the thermocouples within the kidneys, the inefficiency of the array, and the open loop manner in which the array was operated.

The electrical efficiency of the array would usually drop considerably during the first experiment, and during each subsequent experiment due to changes in the electrical impedance of the array elements. Two primary factors were responsible for the observed changes in the electrical impedance of the array elements: The first was a thermally induced impedance drift caused by the array self-heating during sonication. The second impedance shift that occurred from experiment to experiment because the impedance of the array elements did not return to their original impedance after cooling. The impedance shifts made it difficult to accurately control the radiated power delivered to the kidney. Other problems with the array included arcing between elements and water seepage behind the array that reduced the array efficiency in subsequent experiments until the array was repaired and rematched. With a more carefully constructed array, most of the power limiting problems experienced can be avoided.

The acoustical field plots were in good agreement with the theory, and the techniques for heating larger volumes were all functional, though the multiple focusing techniques were the most effective. Overall, phased arrays show considerable potential for improvement over currently used intracavitary ultrasound hyperthermia system.

While phased arrays allow significantly more control over the acoustical field, the current design using half-cylinder radiators still lacks control in the angular direction (around the arc of the array). Additionally, since the cylindrical radiators do not have uniform angular intensities, the angular heating pattern is somewhat degraded, though thermal conduction will probably smooth the resulting temperature distribution. Similar fluctuations in the angular field distributions have been shown for other cylindrical transducers [2], [11]. Radial control could be achieved by dividing the half-cylinder elements into

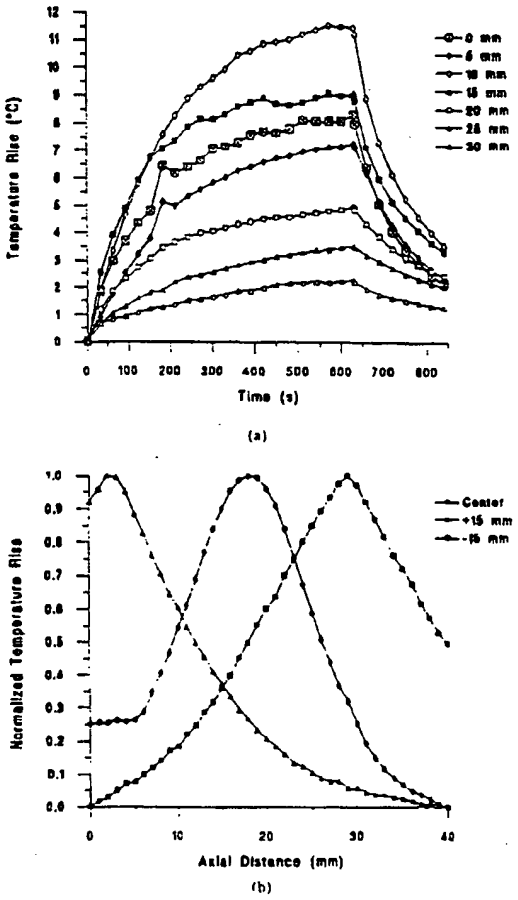

Fig. 9. Temperature profile measured in a perfused kidney using 32 active elements focused 30 mm from the array surface while the kidney was perfused at the rate of 2.9 kg m^{-3} s^{-1} (5 mL min^{-1} flow). The array was positioned 18 mm from the kidney surface. The thermocouple locations indicate the distance from the surface of the kidney. (a) The axial distribution measured 12 mm from the surface of the kidney using a pull-back thermocouple (b) in a separate experiment.

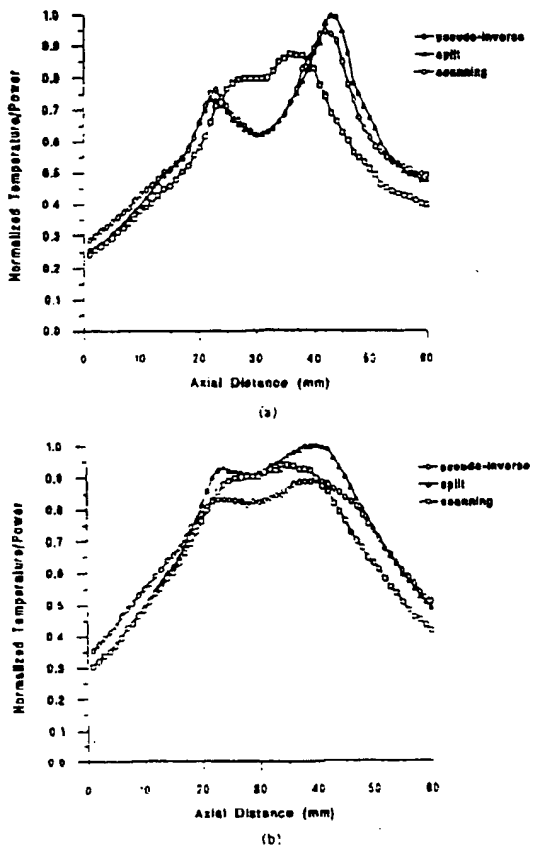

Fig. 10. Normalized temperature/power profiles measured in a perfused kidney for multiple focusing using the pseudo-inverse and split focusing techniques, as well as single-focus scanning. The multiple foci were created 40 mm deep, 10 mm on either side of the central axis while the scanning was done with a single focus 40 mm deep, and scanned 10 mm on either side of the central axis. The measurements were made 6 mm (a) and 15 mm (b) from the surface of the kidney with the array positioned 27 mm from the kidney surface.

pie-shaped subelements and driving each subelement independently. However, this would not only dramatically increase the number of amplifiers, but the resulting subelements would have virtually no inner electrode due to the wall thickness of the element. This would seriously degrade the already low acoustical efficiency of the cylindrical radiators.

A possibly better array design would utilize planer array elements mounted on a rotating platform. By tilting the array back and forth, the same volume could be treated as with the cylindrical radiators. By controlling the acoustic field and output power as a function of tilt angle, 2-D control over the power deposition field can be achieved without requiring additional amplifiers. An additional improvement on the array design would be to increase the operating frequency. While the 500-kHz operating frequency allowed larger element sizes and minimized grating lobe formation, higher frequencies would increase the power absorption in tissues. Since most tumor sites for which this applicator would be used occur near the cavity wall, the deep penetration allowed by the 500-kHz operating frequency is not necessary. The difficulty in increasing the operating frequency is that the element size and center-to-center element spacing would need to decrease as the frequency increased, making array design more difficult.

As a conclusion, the intracavitary, electrically focused array did demonstrate, at practical depths for prostate treatments (about 30 mm), the feasibility of using phased arrays for intracavitary hyperthermia purposes. With a more carefully constructed array, most of the power limiting problems experienced can be avoided. The acoustical field plots were in good agreement with the theory, and the techniques for heating larger volumes were all functional, though the multiple

focusing techniques were the most effective. Overall, phased arrays show considerable improvement over the currently used intracavitary ultrasound hyperthermia system [1]. However, it does not offer power control in the angular direction (around the axis of the applicator) and thus, new designs allowing 3-D control of the power field should be developed before clinical testing.

ACKNOWLEDGMENT

The contents of this article are solely the responsibility of the authors and do not necessarily represent the official views of the National Cancer Institute.

REFERENCES

[1] H. Fosmire, K. Hynynen, G. W. Drach, B. Stea, P. Swift, and J. R. Cassady, "Feasibility and toxicity of transrectal ultrasound hyperthermia in the treatment of locally advanced adenocarcinoma of the prostate," *Int. J. Radiation Oncol. Biol. Phys.*, submitted 1992.

[2] C. J. Diederich and K. Hynynen, "Induction of hyperthermia using an intracavitary multielement ultrasonic applicator," *IEEE Trans. Biomed. Eng.*, vol. 36, no. 4, p. 432, 1989.

[3] ——, "The feasibility of using electrically focused ultrasound arrays to induce deep hyperthermia via body cavities," *IEEE Trans. Ultrason. Ferroelec. Frequency Contr.*, vol. 38, no. 3, pp. 207–219, 1991.

[4] C. A. Cain and S. I. Umemura, "Concentric-ring and sector vortex phased-array applicators for ultrasound hyperthermia," *IEEE Trans. Ultrason. Ferroelec. Frequency Contr.*, vol. UFFC-34, no. 5, pp. 542–551, 1986.

[5] ——, "The sector-vortex phased array: Acoustic field synthesis for hyperthermia," *IEEE Trans. Ultrason. Ferroelec. Frequency Contr.*, vol. 36, no. 2, pp. 249–257, 1989.

[6] E. S. Ebbini, S. I. Umemura, M. Ibbini, and C. A. Cain, "A cylindrical-section ultrasound phased-array applicator for hyperthermia cancer therapy," *IEEE Trans. Biomed. Eng.*, vol. BME-35, no. 5, pp. 561–572, 1988.

[7] E. S. Ebbini and C. A. Cain, "Experimental evaluation of a prototype cylindrical section ultrasound hyperthermia phased-array applicator," *IEEE Trans. Ultrason. Ferroelec. Frequency Contr.*, vol. 38, no. 5, pp. 510–520, 1991.

[8] P. J. Benkeser, L. A. Frizzell, K. B. Ocheltree, and C. A. Cain, "A tapered phased array ultrasound traducer for hyperthermia treatment," *IEEE Trans. Ultrason. Ferroelec. Frequency Contr.*, vol UFFC-34, no. 4, pp. 446–453, 1987.

[9] C. J. Diederich and K. Hynynen, "The development of intracavitary ultrasonic applicators for hyperthermia: A theoretical and experimental study," *Med. Phys.*, pp. 626–634, July-Aug. 1990.

[10] F. Ngo, "Ultrasonic phased-array driver system," M.S. thesis, Univ. of Illinois at Urbana-Champaign, 1988.

[11] C. J. Diederich, "The design and development of intracavitary ultrasound arrays for hyperthermia," Ph.D. dissertation, Univ. of Arizona, Tucson, 1990.

[12] H. Wang and C.A. Cain, "Effect of phase errors on field patterns generated by an ultrasound phased-array hyperthermia applicator," *IEEE Trans. Ultrason. Ferroelec. Frequency Contr.*, vol. 38, no. 5, pp. 521–531, 1991.

[13] ——, "Digital PEP wattmeter and SWR calculator," in *The ARRL Handbook for the Radio Amateur*, B. Hale, Ed. Newington, CT: American Radio Relay League, 1989, pp. 34-10–34-15.

[14] E. S. Ebbini and C. A. Cain, "Multiple-focus ultrasound phased-array pattern synthesis: Optimal driving-signal distributions for hyperthermia," *IEEE Trans. Ultrason. Ferroelec. Frequency Contr.*, vol. 36, no. 5, pp. 540–548, 1989.

[15] E. S. Ebbini, "Deep localized hyperthermia with ultrasound phased arrays using the pseudoinverse pattern synthesis method," Ph.D. dissertation, Univ. of Illinois, Urbana, IL, 1990.

[16] H. F. Stewart, "Ultrasonic measurement techniques and equipment output levels," in *Essentials of Medical Ultrasound*, M. H. Repacholi and D. A. Benwell, Eds. Clifton, NJ: Humana Press, 1982, pp. 77–116.

[17] K. Hynynen, "Acoustic power calibrations of cylindrical intracavitary ultrasound hyperthermia applicators," *Med. Phys.*, vol. 20, pp. 129–134, 1993.

[18] K. R. Holmes, W. Ryan, P. Weinstein, and M. M. Chen, "A fixation technique for organs to be used as perfused tissue phantoms in bioheat transfer studies," in *1984 Advances in Bioengineering*, R. L. Spiker, Ed. New York: American Society of Mechanical Engineers, 1984, pp. 9–10.

[19] K. Hynynen, D. DeYoung, M. Kundrat, and E. Moros, "The effect of blood perfusion rate on the temperature distribution induced by multiple, scanned and focused ultrasonic beams in dogs' kidneys *in vivo*," *Int. J. Hyperthermia*, vol. 5, pp. 485–497, 1989.

[20] J.-E. Damber, A. Bergh, L. Daehlin, V. Petrow, and M. Landstrom, "Effects of 6-methylene progesterone on growth, morphology, and blood flow of Dunning R3327 prostatic andenocarcinoma," *Prostate*, vol. 20, pp. 187–197, 1992.

[21] O. Jonsson, A. Widmark, K. Grankvist, J.-E. Damber, and R. Henriksson, "Effects of clonidine-induced hyperthension on blood flows in prostatic adenocarcinoma (Dunning R3327) and normal tissue," *Prostate*, vol. 20, pp. 225–232, 1992.

Mark T. Buchanan was born in Tucson, AZ, on August 16, 1967. He received the B.S. and M.S. degrees in electrical engineering in 1989 and 1991, respectively, at the University of Arizona.

He is currently continuing his ultrasound research with the Department of Radiology at the Brigham and Women's Hospital in Boston, MA.

Kullervo Hynynen was born in Pyhäntä, Finland, in 1954. He received the M.S. degree from the University of Kuopio, Finland, in 1977, and the Ph.D. degree from the University of Aberdeen, Scotland, in 1982.

From 1982 to 1983, he was a Postdoctoral Research Assistant at the University of Aberdeen, where he was developing a focused ultrasound system for the treatment of tumors. In 1984, he joined the faculty of the University of Arizona, where he reached the rank of Associate Professor of Radiation Oncology. In 1993, he became an Associate Professor of Radiology in Harvard Medical School and Brigham and Women's Hospital. His main research interests include theoretical and experimental development of high power ultrasound devices for therapy, and utilization of ultrasound and MRI to guide, monitor and control the energy exposure.

Attachment II

to Patent Application for

Methods and Apparatus for Delivery of Noninvasive Ultrasound Brain Therapy Through Intact Skull

---

Fan *et al*, "Control of the Necrosed Tissue Volume During Noninvasive Ultrasound Surgery Using a 16-Element Phased Array," Med. Phys., v. 22, pp. 297-308 (1995)

Control of the necrosed tissue volume during noninvasive ultrasound surgery using a 16-element phased array

Xiaobing Fan[a] and Kullervo Hynynen
Department of Radiology, Brigham and Women's Hospital, Harvard Medical School, Boston, Massachusetts 02115

(Received 24 March 1994; accepted for publication 31 October 1994)

Focused high-power ultrasound beams are well suited for noninvasive local destruction of deep target volumes. In order to avoid cavitation and to utilize only thermal tissue damage, high frequencies (1–5 MHz) are used in ultrasonic surgery. However, the focal spots generated by sharply focused transducers become so small that only small tumors can be treated in a reasonable time. Phased array ultrasound transducers can be employed to electronically scan a focal spot or to produce multiple foci in the desired region to increase the treated volume. In this article, theoretical and experimental studies of spherically curved square-element phased arrays for use in ultrasonic surgery were performed. The simulation results were compared with experimental results from a 16-element array. It was shown that the phased array could control the necrosed tissue volume by using closely spaced multiple foci. The phased array can also be used to enlarge a necrosed tissue volume in only one direction at a time, i.e., lateral or longitudinal. The spherically curved 16 square-element phased array can produce useful results by varying the phase and amplitude setting. Four focal points can be easily generated with a distance of two or four wavelengths between the two closest peaks. The maximum necrosed tissue volume generated by the array can be up to sixteen times the volume induced by a similar spherical transducer. Therefore the treatment time could be reduced compared with single transducer treatment.

Key words: phased array, ultrasonic surgery

I. INTRODUCTION

In ultrasound surgery, to avoid cavitation and have a sharp boundary between the tumor and normal tissue, high frequency focused transducers have to be used.[1] The focal spots generated by sharply focused ultrasound transducers are small when compared with the diameter of many tumors. Obviously this type of focus is not efficient to treat large tumors, which would require a large number of exposures to cover the whole target volume. However, in order to accurately treat the target volume close to critical structures, s . focal spots may be required during part of the therapy. Thus, controllable focal spot size is required. The most attractive method to obtain control over the focal spot size is to use phased arrays.

Phased array applicators were introduced to ultrasound hyperthermia cancer therapy in the early 1980's. During the past decade, many efforts have been made to investigate the advantages of phased arrays in hyperthermia, and several phased array applicators have been developed. Phased array applicators can be divided into the following categories: annular or concentric-ring arrays,[2,3] stacked linear-phased arrays,[4] sector-vortex arrays,[5] tapered linear-phased arrays,[5] cylindrical-section arrays,[6] and square-element spherical-section arrays.[7] It was shown that ultrasound phased arrays can provide good control over the heating pattern with flexibility in moving the focus and producing multiple foci. Previous research in ultrasound phased arrays has been concentrated in hyperthermia cancer therapy. Relatively low frequencies (about 0.5 MHz) and small element size (compared to the wavelength) were employed in these studies. The studies on square-element spherical-section arrays emphasized using a large number of elements, up to a few hundred. The main disadvantage associated with using a large number of elements is that the same number of amplifiers and electronic circuits are also required.

The motivation of this article was to demonstrate that a phased array system with a small number of elements can be utilized to provide control over the focal spot size for surgical purposes. The excitation signals of the elements vary in both amplitude and phase. Hence the major task in utilizing phased arrays is to determine the phases and amplitudes needed to produce desired ultrasound fields. The inverse technique introduced by Ebbini and Cain[6] can be used for direct synthesis of ultrasound fields with multiple foci. Several amplitude and phase settings were calculated for different sets of selected control points. The limitation of the number of utilizable control points was also investigated for a given array. Several simplified amplitude and phase settings based on the calculated amplitudes and phases were employed for ultrasound field calculations. These driving signal sets can be utilized, when different focal spot sizes are required for the array proposed here. The transient bioheat transfer equation was employed to estimate the temperature elevation due to the ultrasound power deposition. Then the necrosed tissue volume was predicted by the isothermal dose volume. Computer programs were also used to do a parametric study to investigate the influence of the dimensions and frequency of the array on the necrosed tissue volume.

II. MATERIALS AND METHODS

A. Square-element array with spherical surface

The phased array was made from a spherically curved transducer which was divided into small square elements. The whole array was airbacked. It was constructed from a

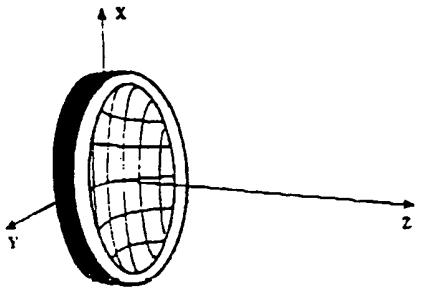

FIG. 1. Configuration of the square-element spherically curved phased array with its coordinate system.

spherically curved PZT4 bowl, having a diameter of 100 mm, a radius of curvature of 130 mm, and a frequency of 1.4 MHz. The bowl was cut into 16 elements, each with a length of 20 mm per side. A 0.3-mm space between the elements was filled with silicone rubber for electrical and mechanical isolation. Each of the elements was connected to an LC matching circuit to match the impedance to 50 Ω and 0°. The array was driven with a custom made 16 channel amplifier (Labthermics, Champaign, Illinois). The phase and amplitude were controlled by RF signals feeding the amplifiers. The driving signals were generated by an in-house manufactured digital circuit.[9] The amplitude and phase of each input signal were digitally controlled with 3-bit resolution in amplitude and 4-bit resolution in phase. The number of elements in each row and each column were the same so that the whole applicator was a square shaped focused transducer. The configuration of the phased array for the experiments is shown in Fig. 1.

B. Ultrasound field measurements

The relative pressure amplitude squared distributions were measured in degassed water using a needle hydrophone (active spot size 1 mm) scanned across the focal region. The needle hydrophone was moved by stepper motors, typically with 0.1-mm steps across the beam. The total acoustic power was measured using a radiation force technique.

C. Computation of ultrasonic fields

Consider an ultrasound phased array with N elements, employed to produce an ultrasonic field in a nonattenuating medium. Assume the coordinate system is defined as in Fig. 1. According to the theory of ultrasonic radiators developed by O'Neil[10] and the principle of superposition of acoustic pressure, the pressure field due to this transducer can be evaluated by the Rayleigh–Sommerfeld integral. The integral is

$$p_m = \frac{j\rho c k}{2\pi} \sum_{n=1}^{N} u_n \int_{S_n} \frac{e^{-jkr_{mn}}}{r_{mn}} dS_n, \tag{1}$$

where $j = \sqrt{-1}$, ρ is the density of medium, c is the speed of sound, k is the real wave number, $u_n = A_n e^{j(\omega t + \theta_n)}$ is the complex excitation source of the nth element with amplitude A_n and phase θ_n, r_{mn} is the distance from a point (x_n, y_n, z_n) on the nth element to the field point of interest (x_m, y_m, z_m), S_n is the area of the nth element.

In ultrasonic surgery, water is used as a coupling medium between the transducer and tissue interface. Water is considered a nonattenuating medium, and tissue a weakly attenuating medium. The effects of attenuation can be satisfactorily described by replacing $e^{-jkr_{mn}}$ with $e^{-jk_c r_{mn}}$ in expression (1), where $k_c = k - j\alpha$ is the complex wave number with attenuation coefficient α.[11,12]

The power deposition for the desired volume is given by

$$Q(x, y, z) = \mu_{abs} \frac{|p_m(x, y, z)|^2}{Z}, \tag{2}$$

where μ_{abs} is the absorption coefficient and $Z = \rho c$ is the impedance of the medium.

D. Inverse technique

The inverse technique can be used to calculate the amplitude and phase settings from selected control points where the desired pressure values are given. Defining

$$h_{mn} = \frac{j\rho c k}{2\pi} \int_{S_n} \frac{e^{-jkr_{mn}}}{r_{mn}} dS_n, \tag{3}$$

then for M field points, expression (1) can be written in matrix notation as

$$P = HU \tag{4}$$

where

$$P = \begin{pmatrix} p_1 \\ p_2 \\ \vdots \\ p_M \end{pmatrix}, \quad H = \begin{pmatrix} h_{11} & h_{12} & \cdots & h_{1N} \\ h_{21} & h_{22} & \cdots & h_{2N} \\ \vdots & \vdots & & \vdots \\ h_{M1} & h_{M2} & \cdots & h_{MN} \end{pmatrix},$$

$$U = \begin{pmatrix} u_1 \\ u_2 \\ \vdots \\ u_N \end{pmatrix}$$

The elements of matrix H are evaluated by numerical integration using expression (3). Equation (4) has two important features. First, if the H matrix is calculated and saved for a desired field, then the pressure field can be evaluated using Eq. (4) instead of Eq. (1) for a given excitation source matrix U. Computation time can be saved by using this method when varying the excitation source over the same calculation volume. Second, for a desired pressure field pattern, i.e., for a given matrix P, the excitation source U can be calculated by

$$U = H^{+} P$$

where H^{+} is the pseudoinverse matrix of H. Usually the total number of control points are much less than the total number

TABLE I. Selected control points used for inverse calculations for 16 square-element spherical curved phased array. The control points are located at $z=129$ mm plane. Note the units for x and y are millimeters.

	x	y	Phase
	1.25	0.0	0.0°
Case	0.0	1.25	0.0°
I	−1.25	0.0	0.0°
	0.0	−1.25	0.0°
	1.25	0.0	0.0°
Case	0.0	1.25	90.0°
II	−1.25	0.0	180.0°
	0.0	−1.25	270.0°
	3.25	0.0	0.0°
Case	0.0	3.25	90.0°
III	−3.25	0.0	180.0°
	0.0	−3.25	270.0°
	5.25	0.0	0.0°
Case	0.0	5.25	90.0°
IV	−5.25	0.0	180.0°
	0.0	−5.25	270.0°
	3.25	0.0	0.0°
	1.62	2.81	60.0°
Case	−1.62	2.81	120.0°
V	−3.25	0.0	180.0°
	−1.62	−2.81	240.0°
	1.62	−2.81	300.0°
	3.25	0.0	0.0°
	2.3	2.3	45.0°
	0.0	3.25	90.0°
Case	−2.3	2.3	135.0°
VI	−3.25	0.0	180.0°
	−2.3	−2.3	225.0°
	0.0	−3.25	270.0°
	2.3	−2.3	315.0°

of excitation sources in this case. The H^* matrix can be found by utilizing single value decomposition.

The control points were selected in a plane at a desired focal position. All the points were evenly distributed on a circle. Since the pressure at a control point is a complex number, both the magnitude and the phase are required to perform the inverse calculations. In selecting control points in this manner, it is natural to make the magnitudes the same for all the points, and the phases either in phase or out of phase so that the phase rotates around the central axis. The latter setup gives destructive interference on the central axis thus, eliminating potential hot spots on the axis.[3] The selected control points used in the inverse calculations are given in Table I.

E. Thermal modeling

An approximate temperature response to the power deposition was predicted by the transient bioheat transfer equation. The differential equation is

$$\rho_t c_t \frac{\partial T}{\partial t} = k_t\left(\frac{\partial^2 T}{\partial x^2} + \frac{\partial^2 T}{\partial y^2} + \frac{\partial^2 T}{\partial z^2}\right) - w c_b (T - T_a) + Q(x,y,z), \quad (5)$$

where T is the temperature at time t, the location (x,y,z), ρ_t is the density of the tissue, c_t is the specific heat of the tissue, k_t is the thermal conductivity of the tissue, w is the blood perfusion rate, c_b is the specific heat of the blood, T_a is the arterial blood temperature, and $Q(x,y,z)$ is the acoustic power deposition rate per unit mass. The thermal response was simulated in a homogeneous medium. A surface temperature of 37 °C on the cube and an initial temperature of 37 °C inside the cube were used as boundary and initial conditions for all of the computations. A numerical finite difference method was employed to solve Eq. (5). Previous studies have shown that there are several parameters which affect the temperature elevation.[13] Temperature elevation has been shown to be almost independent of the blood perfusion rate for short ultrasound pulses.[14] For this reason, ultrasound pulse durations of 1, 5, and 10 s were used in this study. The maximum temperature reached in all simulations was kept the same (80 °C) by adjusting the input power.

F. Thermal dose calculation and necrosed tissue volume estimation

The thermal dose calculation was based on the technique suggested by Sapareto and Dewey.[15] Using this technique, the accumulated thermal dose was calculated at a reference temperature by numerical integration under different temperature profiles. The thermal dose, i.e., equivalent time, at the reference temperature can be evaluated by

$$\text{Dose}(t_{T_{ref}}) = \int_{t=0}^{t=t_{final}} R^{T_{ref}-T(t)}\,dt = \sum_{t=0}^{t=t_{final}} R^{T_{ref}-T_{\Delta t}}\Delta t, \quad (6)$$

where T_{ref} is the reference temperature, $t_{final} = t_{heating} + t_{cooling}$ is the final time, Δt is a small time interval, $T_{\Delta t}$ is the average temperature during time Δt, and R is a parameter given by

$$R = \begin{cases} 0.5, & \text{if } T(t) \geq 43\ ^\circ\text{C} \\ 0.25, & \text{otherwise} \end{cases}$$

The necrosed tissue volume is estimated by the isothermal dose volume surrounded for 240 min at the reference temperature of 43 °C. This technique has been found to be a reasonable model for predicting tissue necroses induced by a spherically curved transducer.[13]

A two layered medium water–tissue was assumed in the simulations. The speed of sound and the density were 1500 m/s and 998 kg/m^3, respectively, for both media. The attenuation coefficient of the tissue was assumed to be 10 Np/m/MHz. The thermal properties of the tissue are given in Table II.

III. RESULTS

A. Comparison of experimental results with simulations

It was necessary to verify the numerical model using the 16 square-element phased array with a spherical surface before relying on the simulations. The experimental and simu-

TABLE II. Thermal properties of the tissue used in the simulations.

Parameter	Value	Units
ρ_t—tissue density	998	kg/m^3
c_t—tissue specific heat	3770	J/kg °C
k_t—tissue thermal conductivity	0.5	W/m °C
w—blood perfusion rate	1	kg/m^3 s
c_b—blood specific heat	3770	J/kg °C
T_a—arterial blood temperature	37	°C

lated profiles of the pressure amplitude squared at the acoustic focus are displayed in Fig. 2. All the data were normalized to 1 by dividing by the maximum pressure amplitude squared for each curve. Figure 2(a) shows the results for the case with uniform excitation sources. There was good agreement between the simulations and experimental results for the main beam. When the array was excited by various phase settings, the simulations reasonably predicted the sidelobe distributions found in the experiments [Figs. 2(b)–2(d)] The maximum power output measured was at least 14 W for each transducer element.

B. Simulation results

The phased array ultrasound transducer used in the experiments was simulated first. A calculation volume of 30 ×30×90 mm^3 was used for this phased array. The axial distance from the center of the transducer to the water–tissue interface was 70 mm. The inverse technique results are shown first. The amplitude and phase settings calculated by the inverse technique corresponding to selected control points are given in Table III (only the first four are shown). The contour plots of power deposition calculated for these array settings are displayed in Fig. 3. For four control points only one focus was produced, which was centered on the

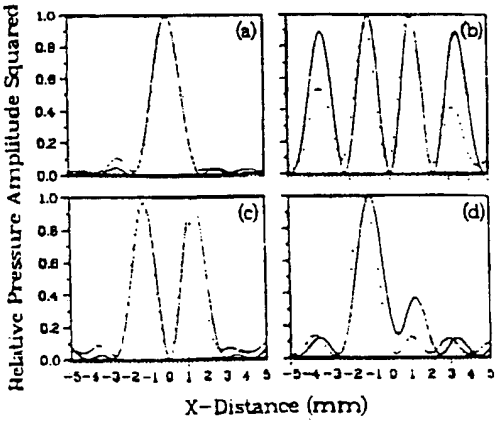

FIG. 2. Relative pressure amplitude squared distribution as a function of lateral distance at the acoustic focus (z = 129 mm). The profile with the dotted line was measured, and the profile with the solid line was simulated. The amplitudes were all the same with phases (a) uniform ... and (d) various.

TABLE III. Phase and amplitude settings calculated with the inverse technique for the 16 square-element spherically curved phased array.

	θ_n				A_n			
	[illegible]	64.2°	64.2°	265.7°	1.0	2.6	2.6	1.0
Case	64.2°	58.1°	58.1°	64.2°	2.6	6.2	6.2	2.6
I	64.2°	58.1°	58.1°	64.2°	2.6	6.2	6.2	2.6
	265.7°	64.2°	64.2°	265.7°	1.0	2.6	2.6	1.0
	119.7°	95.0°	38.0°	29.7°	1.8	1.5	1.5	1.8
Case	128.0°	104.1°	14.1°	5.0°	1.5	1.0	1.0	1.5
II	185.0°	194.1°	284.1°	308.0°	1.5	1.0	1.0	1.5
	209.7°	218.0°	275.0°	299.7°	1.8	1.5	1.5	1.8
	311.9°	212.3°	304.3°	221.9°	1.0	1.0	1.0	1.0
Case	34.3°	114.9°	24.9°	122.3°	1.0	1.0	1.0	1.0
III	302.3°	204.9°	294.9°	214.3°	1.0	1.0	1.0	1.0
	41.9°	124.3°	32.3°	131.9°	1.0	1.0	1.0	1.0
	158.0°	142.4°	59.2°	66.0°	1.1	1.2	1.0	1.1
Case	149.2°	133.2°	42.2°	52.4°	1.0	1.0	1.0	1.2
IV	232.4°	223.2°	313.2°	329.2°	1.2	1.0	1.0	1.0
	248.0°	239.2°	322.4°	338.0°	1.1	1.0	1.2	1.1

axis when the pressure at all of the control points were in phase [Figs. 3(a) and 3(b)]. Four focal spots were obtained if the pressure at the control points had 90.0° phase shifts from one point to another [Figs. 3(c) and 3(d)] Comparing Figs. 3(c) and 3(d) with Figs. 3(e) and 3(f), the peak to peak distance was increased when the control points on a 1.25-mm radius circle increased to a 3.25-mm radius circle. However, if the control points were on a 5.25-mm radius circle, the focal spots were at the same location as Figs. 3(c) and 3(d). The field distributions (not shown here) were very similar to Figs. 3(c) and 3(d) For six control points, six focal spots were obtained at control locations with different patterns [Figs. 3(g) and 3(h)], and two additional focal spots were at the center. When the number of control points increased to eight, the power deposition pattern had the maximum pressure amplitude in front of the focal plane with strong peaks at the water–tissue interface [Figs. 3(i) and 3(j)]. These results were used to select simplified amplitude and phase settings which were then used in necrosed tissue volume simulations (Table IV).

The isothermal doses for tissue necrosis for five amplitude and phase settings are displayed in Fig. 4. Let us consider the ultrasound pulse duration 10-s case (solid line). For the uniform excitation case, the focus was located at a depth of 59 mm from the interface. Based on the 240-min isothermal dose [Figs. 4(a) and 4(b)], the shape of the necrosed tissue volume was close to an ellipsoid. The calculated volume was about 85 mm^3, measuring 3 mm laterally and 18 mm longitudinally. Isothermal doses are also shown in the same figures for the ultrasound pulse durations of 5 and 1 s, where the input power was adjusted so that the maximum temperature was kept at 80 °C. For case I of Table IV, the necrosed tissue length [Fig. 4(c)] was 42 mm, and the width [Fig. 4(d)] was 3.4 mm. The length was more than double and the width was slightly enlarged compared to the uniform excitation case. The computed necrosed tissue volume was about 339 mm^3. Figures 4(e) and 4(f) show case II of Table IV, for

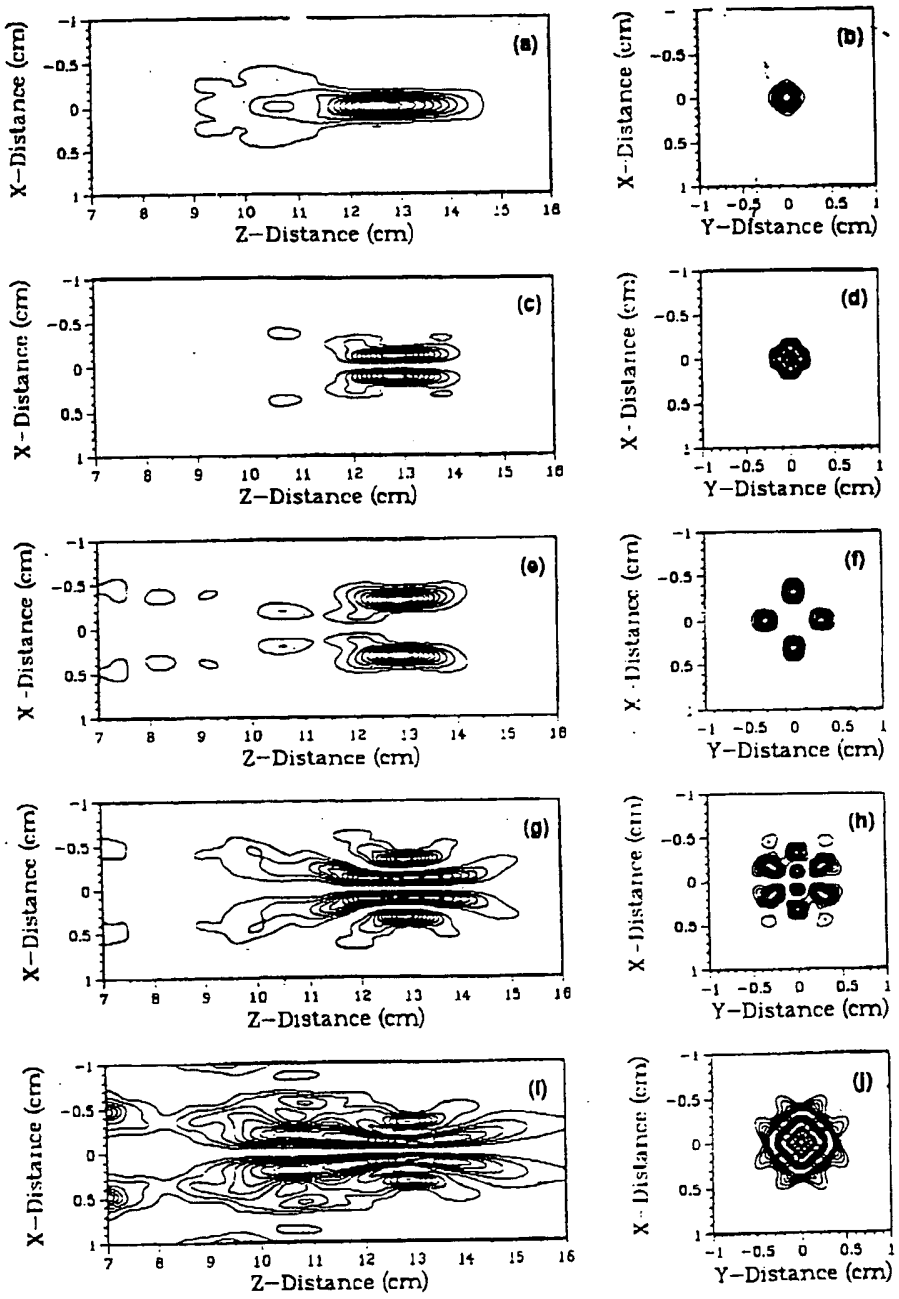

FIG. 3. Contour plots of power deposition for calculated amplitude and phase settings. The contour points used to calculate amplitudes and phases from Table I were (a), (b) case I; (c), (d) case II; (e), (f) case III; (g), (h) case V; and (i), (j) case VI. The figures on the left side are axial plane distributions, and on the right side are focal plane distributions (z = 129 mm).

TABLE IV. The simplified phase and amplitude settings for the 16 square-element spherically curved phased array used in the necrosed tissue volume calculations.

	θ_n				A_n			
	0.0°	0.0°	0.0°	0.0°	1.0	1.0	1.0	1.0
Case	0.0°	0.0°	0.0°	0.0°	1.0	5.0	5.0	1.0
I	0.0°	0.0°	0.0°	0.0°	1.0	5.0	5.0	1.0
	0.0°	0.0°	0.0°	0.0°	1.0	1.0	1.0	1.0
	90.0°	90.0°	0.0°	0.0°	1.0	1.0	1.0	1.0
Case	90.0°	90.0°	0.0°	0.0°	1.0	1.0	1.0	1.0
II	180.0°	180.0°	270.0°	270.0°	1.0	1.0	1.0	1.0
	180.0°	180.0°	270.0°	270.0°	1.0	1.0	1.0	1.0
	270.0°	180.0°	270.0°	180.0°	1.0	1.0	1.0	1.0
Case	0.0°	90.0°	0.0°	90.0°	1.0	1.0	1.0	1.0
III	270.0°	180.0°	270.0°	180.0°	1.0	1.0	1.0	1.0
	0.0°	90.0°	0.0°	90.0°	1.0	1.0	1.0	1.0
	270.0°	240.0°	210.0°	180.0°	1.0	1.0	1.0	1.0
Case	300.0°	90.0°	0.0°	150.0°	1.0	1.0	1.0	1.0
IV	330.0°	180.0°	270.0°	120.0°	1.0	1.0	1.0	1.0
	360.0°	30.0°	60.0°	90.0°	1.0	1.0	1.0	1.0

which the necrosed tissue length and width were 20.8 and 5.1 mm, respectively. The length was slightly longer and the width was almost double compared with the uniform excitation case. Notice that this case is equivalent to the situation in which the phased array had only four elements with sides of 39.4 mm. The calculated necrosed tissue volume was about 377 mm^3. Figures 4(g) and 4(h) indicate that there were four focal points in the power deposition for case III of Table IV. The shortest peak to peak distance was about 4λ, where λ is the wavelength. The whole volume was the summation of the four individual small necrosed tissue volumes which were produced by the four focal points. Each small volume was about the same size as the volume in the uniform excitation case for the 1- and 5-s sonications. For the 10-s sonication a united volume was created with the total volume of 810 mm^3. For the amplitude and phase setting of case IV in Table IV, the power deposition (not shown here) indicated that there were four strong focal points (depth 54 mm) surrounded by four small focal points. The shortest distance between the strong peaks was about 2λ. Simultaneous focusing at these points was performed to enlarge the heated volume compared to the uniform excitation case. The calculated isothermal dose [Figs. 4(i) and 4(j)] from the temperature distribution had a maximum length of 38.5 mm and a maximum width of 7.2 mm, and the necrosed tissue volume was close to 1.4 cm^3.

To illustrate the effect of frequency on necrosed tissue volume production, the isothermal doses for case IV of Table IV with an ultrasound pulse duration 10 s are shown in Figs. 5(a) and 5(b). The calculated volume was $60\times60\times90$ mm^3 for 0.5 MHz, $40\times40\times90$ mm^3 for 1.0 MHz, and $30\times30\times90$ mm^3 for 1.4 and 2.0 MHz. The distance from the transducer to the interface was kept the same (70 mm), while the frequency was varied. The ratio of the necrosed tissue length to width was almost independent of frequency. The size increased as the frequency decreased. The shapes were similar for frequencies of 1 to 2 MHz.

To understand the effect of radius of curvature on the necrosed tissue volume, the isothermal doses for case IV of Table IV, with an ultrasound pulse duration of 10 s and operating frequency of 1.4 MHz are displayed in Figs. 5(c) and 5(d). The distance from the transducer to the interface was varied according to the radius of curvature to maintain a constant focal depth. The necrosed tissue volume increased rapidly along the longitudinal direction toward the interface as the radius of curvature increased. However, the diameter of the necrosed tissue volume increased only slightly in the focal plane.

To show the capability of the phased array to move the focus, contour plots of the power deposition for the maximum displacement are displayed in Fig. 6. The simulation model was the same as the one used to generate Fig. 3. The phase distributions were obtained based on direct calculations, i.e., phase $\theta_n = 2\pi d_n/\lambda$, $n = 1,2,\ldots,N$, where d_n is the distance from the center of the element to a desired focus. Figure 6(a) shows the results for the case with uniform amplitude and phase setting. The focus could be moved 7 mm closer to the interface [Fig. 6(b)], or 7 mm deeper [Fig. 6(c)] compared with Fig. 6(a). Figure 6(d) shows the phased array focus shifted 1.5 mm off the central axis. When larger displacements were attempted, the phase increment between adjacent elements exceeded $\pi/2$. Distributions generated by those phases are no longer single, strongly focused ultrasound fields. Therefore these were the maximum displacements achievable with this array in the sense of keeping the fields in the region of focus similar to those for the uniform excitation case.

Finally, Fig. 7 shows the input power requirements for the uniform excitation and four amplitude and phase settings given in Table IV. For ultrasound pulse durations of 5 or 10 s, the power ranged from 30 to 250 W. For a 1-s pulse, the input power could be as high as 900 W, depending on the amplitude and phase settings.

IV. DISCUSSION

The experimental and simulation results showed that a 16-element phased array can offer significant control over the size and shape of the necrosed tissue volume during ultrasound surgery. The experiments showed that such an array can be constructed and it can deliver enough power for surgical purposes. The simulated and experimental ultrasound field distributions agreed reasonably well. The differences may be due to uneven element size and power output in the phased array as well as measurement errors. Since the peak to peak distance was only a few millimeters, the ultrasound detector may contribute some measurement errors. The simulation model accurately predicted the locations of sidelobes and main beams except that it over predicted the magnitude of the sidelobes. When adjacent elements of a phased array are very close to each other, the mutual coupling between the elements would have an effect on the ultrasound field. The difference between the sidelobes in the experiments and the simulations may be due to the lack of such crosstalk in the calculations.

The above results proved that the large element spherically curved phased array can enlarge the necrosed tissue

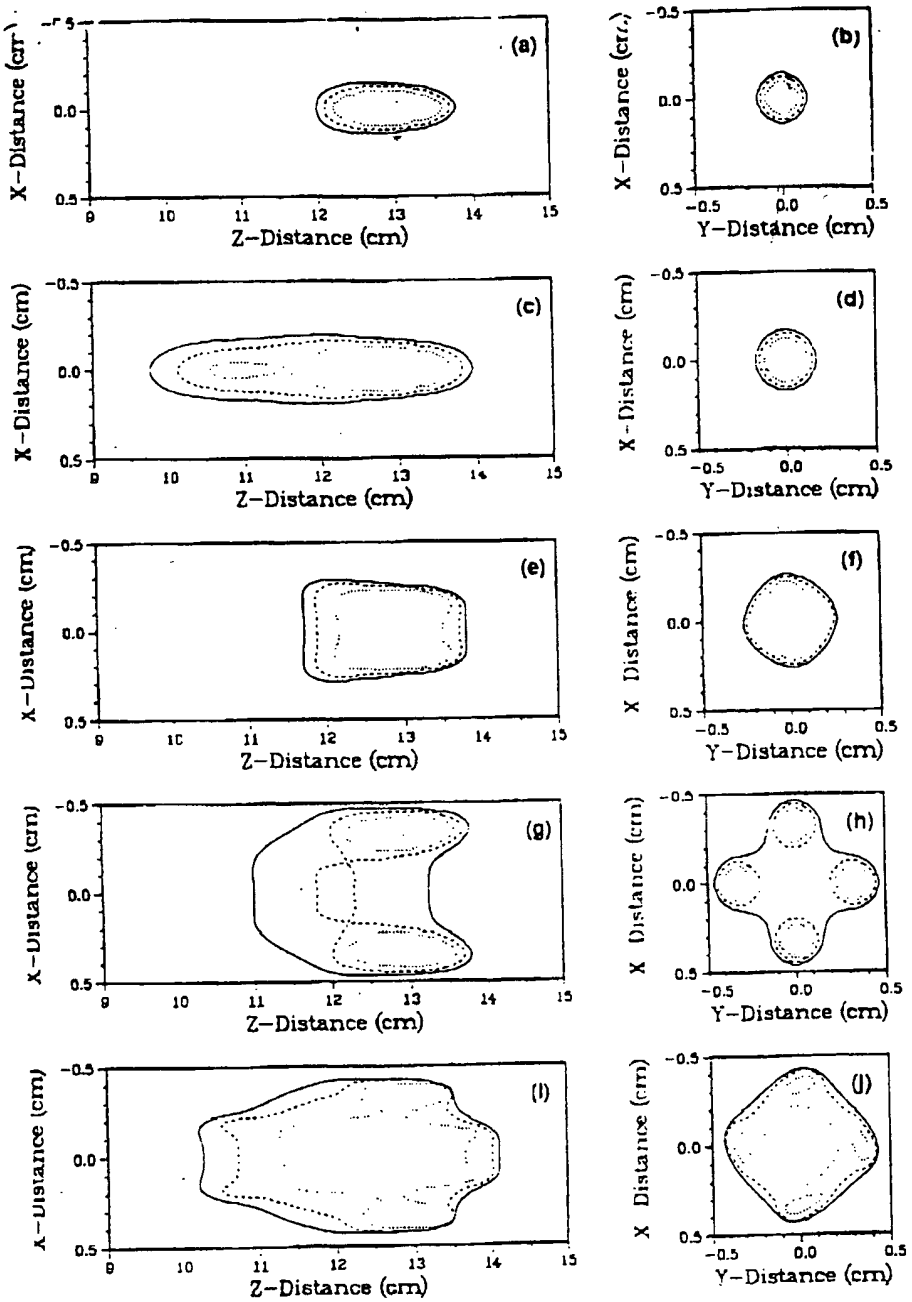

FIG. 4. Isothermal doses for the uniform excitation case (a), (b) and the amplitude and phase settings in Table IV: (c), (d) case I; (e), (f) case II; (g), (h) case III; and (i), (j) case IV. The figures on the left side are axial plane distributions, and on the right side are focal plane distributions [(b) $z = 129$ mm, (d) $z = 128$ mm, (f) $z = 126$ mm, (h) $z = 129$ mm, and (j) $z = 124$ mm]. The ultrasound pulse durations used in the thermal dose calculations were 10 s (solid line), 5 s (dashed line), and 1 s (dotted line).

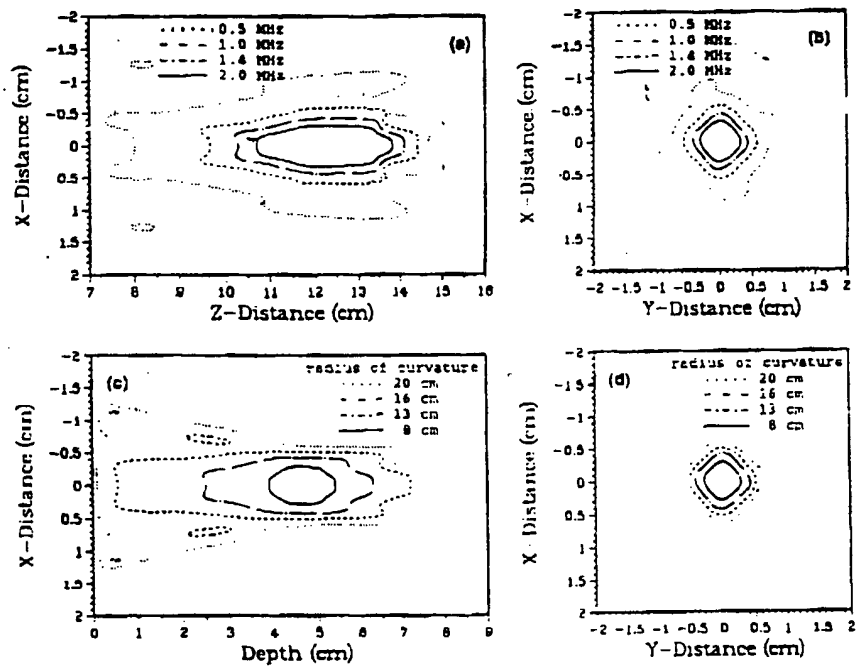

FIG. 5. The isothermal dose for case IV of Table IV with various frequencies (a), (b), and with various radii of curvature (c), (d). The ultrasound pulse duration used in the thermal dose calculations was 10 s. The distance from the transducer to the interface was 130, 100, 75, and 32 mm for radii of curvature of 200, 160, 130, and 80 mm, respectively. (a), (c) is axial plane distribution, and (b), (d) is the focal plane distribution.

volume. The phased array can also enlarge the necrosed tissue volume in only one direction at a time, if desired. It is important to be able to control the focal spot size so that a large tumor could be treated in a reasonable time. The construction of the whole system was relatively simple due to the small number of elements. The 16-element phased array can also shift the focus off the central axis or move the focus along the central axis. However the distance is limited to ± 1.5 mm laterally and 14 mm in the axial direction. In moving the focus along the central axis, the array is similar to a concentric-ring array with two rings. Theoretically, the maximum phase increment between adjacent elements is π. Therefore, the maximum possible phase difference between the smallest and largest phases is π when moving the focus along the central axis. From geometric considerations, this phase difference produces displacements along the central axis of up to 23 mm (10 mm closer, 13 mm deeper). In shifting the focus sideways, it is similar to a cylindrical-section array with four elements. The maximum possible phase difference between the smallest and largest phases is 3π for shifting the focus sideways. Geometrically, this phase difference shifts the focus ± 3.4 mm laterally. However, the simulations showed that the phase increment between the adjacent elements should be less than $\pi/2$ to generate a single strongly focused ultrasound field.

The 16-element phased array can generate four focal points with a peak to peak distance as short as two wavelengths. The maximum distance between the closest peaks is limited to about four wavelengths. When the four control points were on a circle of radius 5.25 mm, the phase increment between adjacent elements exceeded π for this array. Therefore, it is physically impossible to use the phase and amplitude setting obtained by inverse techniques to produce the four focal spots at the control points. Although Eq. (4) represents an underdetermind system, it produced a solution at the control points. When multiple foci are separated by distances larger than 4.6 mm, the necrosed tissue volume becomes a few individual smaller volumes, which are not united for short ultrasound pulse durations.

By decreasing the frequency, the necrosed tissue volume can be enlarged because the focal spot increases due to the increased wavelength. But the ratio of the necrosed tissue length to the width was kept almost the same. As the radius of curvature is increased, the necrosed tissue volume can also be enlarged. The necrosed tissue volume is increased mainly in the axial direction. This agrees with previous experience using single element spherically curved transducers.[13]

Phased arrays require more input power than similar single focused transducers to reach the same temperature level for the same ultrasonic pulse duration due to increased

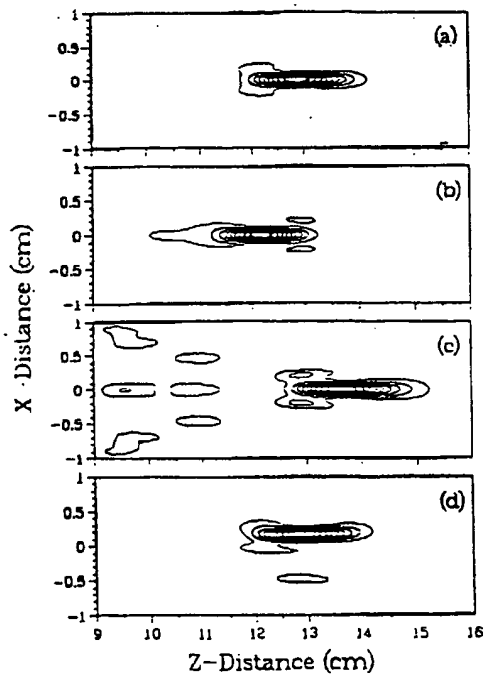

FIG. 6. Contour plots of power deposition for various amplitude and phase settings. (a) is the uniform excitation case. The axial distance from the transducer to the focus was (a) 129 mm, (b) 122 mm, (c) 136 mm, and (d) 129 mm, shifted 1.5 mm.

focal spot size. The test array measurements showed that therequired power levels can be generated in practice at least 5- and 10-s exposures and thus, the proposed technique is feasible.

In order to obtain the desired field pattern, several field control points are necessary to perform the inverse calculations. However, the number of utilizable field control points is limited by the number of phased array elements. Hence the number of field patterns that produce significantly different shapes or sizes of the measured volume is limited. Although only few amplitude and phase settings were presented in this study, the results provided information which could aid in planning ultrasonic surgery using a phased array system with a small number of elements. These results have not been optimized; nevertheless they illustrate the feasibility and range of focal size and shape obtainable with a 16-element array. The calculations and experiments can be used to obtain a set of different focal spots for a given array. This limited number of focal spots can then be utilized to optimally cover the target volume in minimum time. The minimization of the duration of the treatment is an important factor for controlling the cost of the procedure, especially when MRI is used to guide and monitor the treatment.[16] If more control over the field pattern is required then an array with a larger number of elements is required. Such an array could also be used

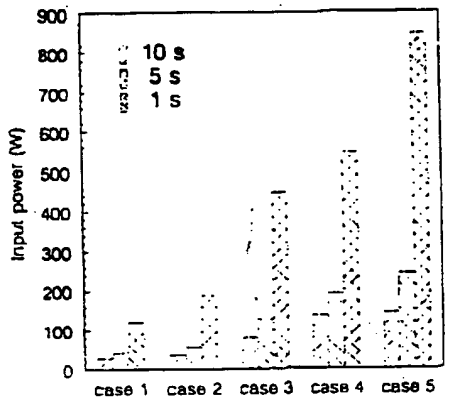

FIG. 7. The input power requirement to reach the same temperature level at the end of ultrasound pulses for various cases. Case 1 is for the uniform excitation case. case 2–5 are corresponding to the amplitude and phase settings of case I–IV in Table IV.

to compensate for the effect of tissue nonuniformities which may distort the focal pattern.[11,12]

ACKNOWLEDGMENT

This study was supported by NCI Grant No. CA 46627.

[a]Department of Electrical and Computer Engineering, University of Arizona, Tucson, AZ 85721

[1]K. Hynynen, "The threshold for thermally significant cavitation in dog's thigh muscle *in vivo*," Ultrasound Med. Biol. 17, 157–169 (1991).

[2]J. P. Do-Huu and P. Hanemann, "Annular array transducer for deep acoustic hyperthermia," Ultrasonics Symp. Proc. IEEE-81 CH 1689-9, 705–710 (1981).

[3]K. B. Ocheltree, P. J. Benkeser, L. A. Frizzell, and C. A. Cain, "An ultrasonic phased array applicator for hyperthermia," IEEE Trans. Sonics Ultrason., SU-31, 526–531 (1984).

[4]C. A. Cain and S. Umemura, "Concentric-ring and sector-vortex phased array applicators for ultrasound hyperthermia," IEEE Trans. Microwave Theory Tech., MTT-34, 542–551 (1986).

[5]P. J. Benkeser, L. A. Frizzell, K. B. Ocheltree, and C. A. Cain, "A tapered phased array ultrasound transducer for hyperthermia treatment," IEEE Trans. Ultrason. Ferroelec. Freq. Contr. UFFC-34, 446–453 (1987).

[6]E. S. Ebbini, S. Umemura, M. Ibbini, and C. A. Cain, "A cylindrical-section ultrasound phased-array applicator for hyperthermia cancer therapy," IEEE Trans. Ultrason. Ferroelectr. Freq. Contr. 35, 561–572 (1988).

[7]E. Ebbini and C. A. Cain, "A spherical-section ultrasound phased array applicator for deep localized hyperthermia," IEEE Trans. Biomed. Eng. BME-38, 634–643 (1991).

[8]E. Ebbini and C. A. Cain, "Multiple-focus ultrasound phased-array pattern synthesis: Optimal driving-signal distributions for hyperthermia," IEEE Trans. Ultrason. Ferroelectr. Freq. Contr. 36, 540–548 (1989).

[9]M. Buchanan and K. Hynynen, "Design and experimental evaluation of intracavitary ultrasound phased array systems for hyperthermia," IEEE Trans. Biomed. Eng. BME-41, 1178–1187 (1994).

[10]H. T. O'Neil, "Theory of focusing radiators," J. Acoust. Soc. Am. 21, 516–526 (1949).

[11]X. Fan and K. Hynynen, "The effect of wave reflection and refraction at soft tissue interfaces during ultrasound hyperthermia treatments," J. Acoust. Soc. Am. 91, 1727–1736 (1992).

[12]X. Fan and K. Hynynen, "The effects of curved tissue layers on the

power deposition patterns of therapeutic ultrasound beams," Med. Phys. 21, 25–34 (1994).
[13]C. Damianou and K. Hynynen, "The effect of various physical parameters on the size and shape of necrosed tissue volume during ultrasound surgery," J. Acoust. Soc. Am. 95, 1641–1649 (1994).
[14]B. E. Billard, K. Hynynen, and R. B. Roemer, "Effects of physical parameters on high temperature ultrasound hyperthermia," Ultrasound Med. Biol. 16, 409–420 (1990).
[15]S. A. Sapareto and W. C. Dewey, "Thermal dose determination in cancer therapy," Int. J. Radiat. Oncol. Biol. Phys. 10, 787–800 (1984).
[16]K. Hynynen, A., Darkazanli, E., Unger, and J. Schenck, "MRI-guided noninvasive ultrasound surgery," Med. Phys. 20, 107–115 (1993).

1. An apparatus for delivering ultrasound through the skull to the brain of a patient, the apparatus comprising

A. a plurality of transducers,

B. an excitation source for driving the plurality of transducers to generate and transmit ultrasound through the skull to induce cavitation at least at a selected region of the brain,

C. the excitation source driving at least selected transducers at differing phases with respect to one another.

2. An apparatus according to claim 1, wherein

A. the excitation source drives each of the selected transducers at a phase that compensates for a phase shift effected by the skull in the ultrasound generated and transmitted to the selected region by that transducer,

B. so that the ultrasound generated by the selected transducers arrive substantially in phase with one another at the selected region.

3. An apparatus according to claim 2, wherein the excitation source drives each of the selected transducers at a phase so that the ultrasound generated by the selected transducers arrive at phases within 90° of one another at the selected region.

4. An apparatus according to claim 2, wherein the excitation source drives each of the selected transducers at a phase so that the ultrasound generated by the selected transducers arrive at phases within 45° of one another at the selected region.

5. An apparatus according to claim 2, wherein the excitation source drives each of the selected transducers at a phase so that the ultrasound generated by the selected transducers arrive at phases within 20° of one another at the selected region.

6. An apparatus according to claim 1, wherein the excitation source drives the plurality of transducers to deliver ultrasound to the selected region at a frequency ranging from 0.01 MHz to 10 MHz.

7. An apparatus according to claim 6, wherein the excitation source drives the plurality of transducers to deliver ultrasound to the selected region at a frequency ranging from 0.1 MHz to 2 MHz.

8. An apparatus according to claim 6, wherein the excitation source drives the plurality of transducers to deliver ultrasound to the selected region at a sonication duration ranging from 100 nanoseconds to 30 minutes.

9. An apparatus according to claim 8, wherein the excitation source drives the plurality of transducers to deliver ultrasound to the selected region with continuous wave operation.

10. An apparatus according to claim 9, wherein the excitation source drives the plurality of transducers to deliver ultrasound to the selected region with burst mode operation, where burst mode repetition varies from 0.01 Hz to 1 MHz.

11. An apparatus for delivering ultrasound through the skull to the brain of a patient, the apparatus comprising

A. an ultrasound transducer,

B. an excitation source for driving the transducer to generate and transmit ultrasound through the skull to induce cavitation at least at a selected region of the brain.

12. An apparatus according to claim 11, wherein the excitation source drives the transducer to deliver ultrasound to the selected region at a frequency ranging from 20 kHz to 10 MHz.

13. An apparatus according to claim 6, wherein the excitation source drives the plurality of transducers to deliver ultrasound to the selected region at a frequency ranging from 0.02 MHz to 10 MHz.

14. An apparatus according to claim 13, wherein the excitation source drives the plurality of transducers to deliver ultrasound to the selected region at a sonication duration ranging from 100 nanoseconds to 30 minutes.

15. An apparatus according to claim 13, wherein the excitation source drives the plurality of transducers to deliver ultrasound to the selected region with continuous wave operation.

16. An apparatus according to claim 15, wherein the excitation source drives the plurality of transducers to deliver ultrasound to the selected region with burst mode operation, where burst mode repetition varies from 0.01 Hz to 1 MHz.

17. A method for delivering ultrasound through the skull to the brain of a patient, the apparatus comprising the steps of

A. placing a plurality of transducers in the vicinity of an exterior surface of the patient's skull,

B. driving the plurality of transducers to generate and transmit ultrasound through the skull to induce cavitation at least at a selected region of the brain,

C. the driving step including driving at least selected transducers at differing phases with respect to one another.

18. A method according to claim 17, wherein step (C) includes driving each of the selected transducers at a phase that compensates for a phase shift effected by the skull in the ultrasound generated and transmitted to the selected region by that transducer, such that the ultrasound generated by the selected transducers arrive substantially in phase with one another at the selected region.

19. A method according to claim 18, wherein step (C) includes driving each of the selected transducers at a phase so that the ultrasound generated by the selected transducers arrive at phases within 90° of one another at the selected region.

20. A method according to claim 18, wherein step (C) includes driving each of the selected transducers at a phase so that the ultrasound generated by the selected transducers arrive at phases within 45° of one another at the selected region.

21. A method according to claim 18, wherein step (C) includes driving each of the selected transducers at a phase so that the ultrasound generated by the selected transducers arrive at phases within 20° of one another at the selected region.

22. A method according to claim 17, wherein step (B) includes driving the plurality of transducers to deliver ultrasound to the selected region at a frequency ranging from 0.02 MHz to 10 MHz.

23. A method according to claim 17, wherein step (B) includes driving the plurality of transducers to deliver ultrasound to the selected region at a frequency ranging from 0.1 MHz to 2 MHz.

24. A method according to claim 17, wherein step (B) includes driving the plurality of transducers to deliver ultrasound to the selected region at a sonication duration ranging from 100 nanoseconds to 30 minutes.

25. A method according to claim 17, wherein step (B) includes driving the plurality of transducers to deliver ultrasound to the selected region with continuous wave operation.

26. A method according to claim 17, wherein step (B) includes driving the plurality of transducers to deliver ultrasound to the selected region with burst mode operation, where burst mode repetition varies from 0.01 Hz to 1 MHz.

27. A method for delivering ultrasound through the skull to the brain of a patient, the apparatus comprising

A. placing an ultrasound transducer in a vicinity of an exterior surface of the patient's skull,

B. driving the transducer to generate and transmit ultrasound through the skull to induce cavitation at least at a selected region of the brain.

28. A method claim 27, wherein step (B) includes driving the transducer to deliver ultrasound to the selected region at a frequency ranging from 0.02 MHz to 10 MHz.

29. A method according to claim 28, wherein step (B) includes driving the plurality of transducers to deliver ultrasound to the selected region at a frequency ranging from 0.1 MHz to 2 MHz.

30. A method according to claim 29, wherein step (B) includes driving the plurality of transducers to deliver ultrasound to the selected region at a sonication duration ranging from 100 nanoseconds to 30 minutes.

31. A method according to claim 30, wherein step (B) includes driving the plurality of transducers to deliver ultrasound to the selected region with continuous wave operation.

32. A method according to claim 31, wherein step (B) includes driving the plurality of transducers to deliver ultrasound to the selected region with burst mode operation, where burst mode repetition varies from 0.01 Hz to 1 MHz.

33. An apparatus for delivering ultrasound through the skull to the brain of a patient, the apparatus comprising

A. a plurality of transducers arranged in a two-dimensional array, and

B. an excitation source for driving the plurality of transducers to generate and transmit ultrasound through the skull to induce cavitation at least at a selected region of the brain.

34. An apparatus according to claim 33, wherein the plurality of transducers are arranged in an array having any of a substantially circular and a substantially annular cross-section.

35. An apparatus according to claim 34, wherein the plurality of transducers are arranged in an array having a substantially circular cross-section.

36. An apparatus according to claim 34, wherein the plurality of transducers are at least one of (i) mounted in, and (ii) separated from one another by, a damping agent.

37. An apparatus according to claim 36, wherein the damping agent is any of a natural or synthetic rubber.

38. An apparatus according to claim 34, wherein the excitation source drives at least selected transducers at differing phases with respect to one another.

39. An apparatus according to claim 1, wherein excitation source drives each of the selected transducers at a phase that compensates for a phase shift effected by the skull in the ultrasound generated and transmitted to the selected region by that transducer, so that the ultrasound generated by the selected transducers arrive substantially in phase with one another at the selected region.

40. A method for delivering ultrasound through the skull to the brain of a patient, the apparatus comprising the steps of

A. placing a plurality of transducers in the vicinity of an exterior surface of the patient's skull,

B. driving each of at least selected transducers generate and transmit ultrasound through the skull, and determining a phase shift effected by the skull in ultrasound generated and transmitted by each such transducer,

C. driving the plurality of transducers, together, to generate and transmit ultrasound through the skull to induce cavitation at least at a selected region of the brain,

D. the driving step including driving at least selected the transducers at phases determined in accord with step (B) so that the ultrasound generated by at least the selected transducers arrive substantially in phase with one another at the selected region.

42. A method according to claim 40, wherein the selected region ranges from 1 mm^3 - 1 cm^3 in volume.